



Recent advances on photocatalytic CO₂ reduction using CeO₂-based photocatalysts: A review

Khondaker Afrina Hoque ^{a,b,*}, Sharmin Ara Sathi ^{a,c}, Farjana Akter ^a, Tania Akter ^a, Tahsin Ahmed ^a, Wahid Ullah ^a, Kazi Arafafin ^a, Mohammad Sayadur Rahaman ^a, Hossain M. Shahadat ^a, Abu Bin Imran ^{b,**}, Al-Nakib Chowdhury ^{b,***}

^a Department of Chemistry, Comilla University, Cumilla 3506, Bangladesh

^b Department of Chemistry, Bangladesh University of Engineering and Technology (BUET), Dhaka 1000, Bangladesh

^c School of Chemistry and Molecular Bioscience (SCMB), University of Wollongong, Wollongong, NSW 2500, Australia

ARTICLE INFO

Keywords:

Photocatalytic reduction
Semiconductor
Doping
Heterojunction
Catalyst
Nanocomposites

ABSTRACT

Efforts to combat global warming and energy-related issues involve the solar-driven reduction of CO₂ into worthy fuels and substances. However, the stable nature of CO₂ demands high energy input for transformation. CO₂ reduction using semiconductor materials activated by sunlight is gaining attention for its eco-friendly and economically viable nature. Despite progress, many solar-active catalysts for CO₂ photoreduction encounter challenges like low efficiency and uncontrollable selectivity. The commonly used rare earth oxide ceria (CeO₂) has low sunlight absorption, necessitating changes such as metal-nonmetal doping oxygen vacancy creation, the addition of co-catalysts, and the development of binary, ternary, Z-scheme, and S-scheme heterostructures to improve its use in visible light. Although there has been considerable research on CeO₂ modifications, there is a lack of comprehensive study regarding their characteristics and the precise photochemical reduction mechanisms. This review aims to bridge this gap by thoroughly examining recent breakthroughs in CeO₂-based photo reductants for CO₂ reduction. It focuses on the synthetic techniques of photocatalysts and CO₂ reduction processes, assesses photoactivity enhancement strategies, investigates underlying mechanisms, and addresses the factors influencing CO₂ reduction, efficiencies and selectivity. Finally, the review concludes by offering insights into future challenges and prospects, guiding upcoming research toward sustainable and efficient CO₂ reduction strategies.

1. Introduction

Environmental contamination has been deteriorating since the 18th century, significantly adversely affecting nature, society, and the economy. This is mainly due to the fast population growth and extensive use of petroleum and coal. Emissions of greenhouse gases, including CO₂, are continuously rising. Soil erosion, deforestation, and the use of fossil fuels, particularly natural gas, coal, and oil, are all human-caused sources of greenhouse gas emissions. Because of their ability to produce a greenhouse effect, these gases are primarily responsible for global warming. Since the preindustrial period, the average temperature has increased by approximately one degree Celsius, which is expected to continue. CO₂, one of the major released chemicals, has contributed to climate change due to its consistent annual atmospheric growth [1–9].

Rising sea levels, shifting tides, and extreme weather are only a few of the climatic concerns it has generated, all of which risk human civilization's long-term existence. The fast expansion of sustainable power sources is a method for resolving the growing tension between environmental damage and resource constraints, which are major issues confronting the world today [10–17].

CO₂ could be a potential source of valuable fuels like formic acid that can be converted by theoretically unlimited solar energy [18,19]. It is a highly stable chemical as it contains carbon-oxygen double bonds ($\sim 750 \text{ kJ mol}^{-1}$) whose dissociation energy value is larger than carbon-hydrogen ($\sim 430 \text{ kJ mol}^{-1}$) and carbon-carbon ($\sim 336 \text{ kJ mol}^{-1}$) single bonds. This suggests a significant amount of energy is required to break CO₂ and convert it into other chemicals [20,21]. Furthermore, given that CO₂ contains carbon in its highest oxidation state, the

* Corresponding author at: Department of Chemistry, Comilla University, Cumilla 3506, Bangladesh.

** Corresponding authors.

E-mail addresses: khafrina@cou.ac.bd (K.A. Hoque), abimran@chem.buet.ac.bd (A.B. Imran), nakib@chem.buet.ac.bd (A.-N. Chowdhury).

commonly accepted explanation for the bent configuration of CO₂ involves a transformation from a linear structure. This bent configuration facilitates the reduction of CO₂ through various processes, including CO₂ methanation (CO₂ + 4 H₂ → CH₄ + 2 H₂O), CO₂ dissociation (CO₂ → CO + O), and methanol synthesis (CO₂ + 3 H₂ → CH₃OH + H₂O) [22].

Several chemical, biological, electrochemical, thermochemical, and photochemical processes have recently been reported to convert CO₂ into alcohols and light hydrocarbons [19,23–26]. Among many approaches, CO₂ photocatalytic reduction has shown to be an attractive alternative technology if it is possible to provide cleaner petrol gases for fuel and industrial use. This is performed by using sunlight to activate semiconductor materials, reducing gaseous pollutants. The most promising approach is to absorb carbon dioxide and transform it into energy-rich compounds such as CO, methanol, formaldehyde, methane, and other valuable chemicals [19,23–25].

Photocatalysis is a change in the rate of a photochemical reaction produced by activating a photocatalyst (a semiconductor) with artificial or natural light (in the ultraviolet or visible spectrum). This technology is both cost-effective and environmentally friendly. This procedure uses a photocatalyst, generally a semiconductor exposed to light with an energy equivalent to or greater than the bandgap. Although several solar-active catalysts for CO₂ photoreduction have been identified, the bulk of them have difficulties with instability, uncontrolled selectivity, decreased conversion rate, and insufficient suppression of competing H₂ evolution processes (HER) in the presence of water [27,28]. Consequently, developing highly active photocatalytic devices for CO₂ reduction with high conversion efficiency and selectivity remains an ongoing challenge. CeO₂ is a semiconductor commonly used in various, including solar cells [29], fuel cells [30], and oxygen sensors [31]. It is seen as a viable choice due to its excellent chemical stability, ability to store and release oxygen, and non-toxicity. Interestingly, CeO₂ is cheaper than lanthanum oxide, and its price is projected to decrease dramatically by 2030. [32].

CeO₂ has been reported as an excellent photocatalyst in previous studies because of its high oxygen storage capacity and abundance of oxygen vacancies (Vo), reversible Ce³⁺/Ce⁴⁺ couples, resistance to photocorrosion, and other favorable catalytic properties [33].

Moreover, CeO₂'s potential performance for the photocatalytic CO₂ process is not inferior to that of other well-known semiconductor materials, like TiO₂ [34,35] ZnO [36,37] and transition metal oxides (i.e., In₂O₃ [38], La₂O₃ [39], WO₃ [40], and others (i.e. La₂Ti₂O₇ [41], CoAlLa-LDH [36,42]). Several recent studies have documented the effectiveness of CeO₂ in reducing and converting CO₂. The yield rates for CO, CH₄, and CH₃OH can reach 15.2 μmolg⁻¹h⁻¹, 3.8 μmolg⁻¹h⁻¹, and 16.3 μmolg⁻¹h⁻¹, respectively [43].

According to Tahir and Amin (2017), this finding is equivalent to the typical photocatalyst TiO₂, which generates CO and CH₄ at 12 μmolg⁻¹h⁻¹ and 0.46 μmolg⁻¹h⁻¹, respectively. Like TiO₂, ZnO is a common catalyst in photocatalytic CO₂ conversion. Its 3.2 eV band gap limits its ability to absorb light to the wavelength below 387 nm [36,37]. According to studies by Nie and colleagues [36,37] and Ali and colleagues [36,37], the ability to make CH₃OH from pure ZnO material is less than that of CeO₂. It is 16.3 times less likely to do so. One of the most appealing value-added goods is CH₃OH, which is also convenient to use and store. Consequently, it is also thought that a photocatalyst that can transform CO₂ into CH₃OH would efficiently aid the process.

However, because of its large bandgap of 2.8–3.1 eV, the n-type CeO₂ semiconductor can only absorb a limited amount of solar spectrum energy up to 400 nm in the visible and less than 5 % in the UV [44]. As a result, there are constraints on the usage of CeO₂. Surface photosensitization has improved the amount of visible light that may be employed over CeO₂, as well as other approaches such as element doping, solid-solution synthesis, associated semiconductors, and noble metal deposition.

Researchers are pretty interested in these modifications and changes, but their properties and response processes are poorly understood. Until

recently, most studies have not offered a detailed description of the specific mechanisms of each heterojunction after doping, nor have they provided a current state-of-the-art analysis of both undoped and doped CeO₂. While a review highlights recent advances in photocatalytic CO₂ reduction by CeO₂-based photocatalysts [45], a comprehensive study encompassing their design, fabrication, photoreduction mechanisms, characterization techniques, band gap modification, comparable efficiency, selectivity for reduction products, limitations, challenges, and prospects is unavailable. To fill this gap, the present review will examine recent advances in photocatalytic CO₂ reduction using CeO₂ photocatalysts. The review describes how CeO₂ semiconductors exposed to light increase CO₂ reduction. It also critically examines various enhancement strategies, such as metal/nonmetal doping, oxygen vacancy formation, binary/ternary nanocomposites, heterojunctions, S-scheme, and Z-scheme heterojunction formation, which are used to increase the photocatalytic activity of CeO₂-based materials by modifying their band gap. The review provides insight into the underlying mechanism processes, comparative efficiencies, and selectivity for CO₂ reduction products by conducting an in-depth review of research articles, synthesis methods, photoreduction techniques, factors affecting photoreduction products, and experimental data. Finally, this article provides insights on current and future aspects regarding photocatalysts based on CeO₂ for CO₂ reduction to provide a thorough overview and guide future research efforts toward sustainable and efficient CO₂ usage.

2. The fundamentals of photocatalytic CO₂ reduction over CeO₂ photocatalysts

There are three critical steps to the photocatalytic CO₂ reduction process. The first step generates electron-hole (e⁻h⁺) pairs, which migrate independently to the photocatalyst particle's surface in the second stage. In the last step, holes and electrons oxidize H₂O to produce O₂ and convert CO₂ to fuel. During the second and final steps, recombination may burn many electrons and holes [21,45–48].

Fig. 1 depicts the photoreduction process by which CeO₂ turns CO₂ into fuel. Semiconductors have distinct energy levels, and the placement of the energy band affects their photocatalytic ability. The O-2p to Ce-4f transition results in a strong absorption of CeO₂ in the 400–500 nm region [49]. According to previous research [50–56], the conduction band (CB) of CeO₂ has a lowermost energy of about –0.4 eV. In contrast, its valence band (VB) has a top energy of approximately 2.5 eV, with a band gap of 2.8–3.1 eV compared to a normal hydrogen electrode (NHE).

When sunlight strikes the CeO₂ semiconductor, the VB electron absorbs a photon (> Eg) and migrates to CB in a femtosecond. This leaves VB with an equal number of holes (h⁺). The surface of CeO₂ undergoes redox reactions in which CO₂ is converted into fuels via photogenerated e⁻ and h⁺ transfer. Table 1 shows that the photocatalytic reduction of CO₂ includes extensive chemical pathways and activities, such as a multi-electron reduction activity with a large energy gap, CO₂ adsorption, and complex activation contributed by proton.

The efficiency and effectiveness of catalyst materials are not limited to their band gap when exposed to the proper quantity of light or to preventing e⁻ and h⁺ recombination by material modification. Other factors include the final product's NHE potential, surface area, deposition process, and particle size. These element's efficiency and electron and hole recombination limitations may be improved to yield higher photocatalytic activity in the future [60].

2.1. Metal or nonmetal doped CeO₂

Although the mesostructure can improve CO₂ adsorption, the rapid combination of light-induced electron and hole pairs for CeO₂ limits the photocatalytic CO₂ conversion efficiency, especially when exposed to visible spectra. Enhancing the efficacy of semiconductor photocatalysts may be achieved by using foreign ion doping, which speeds up the separation of charges and expands the photoexcitation's energy range.

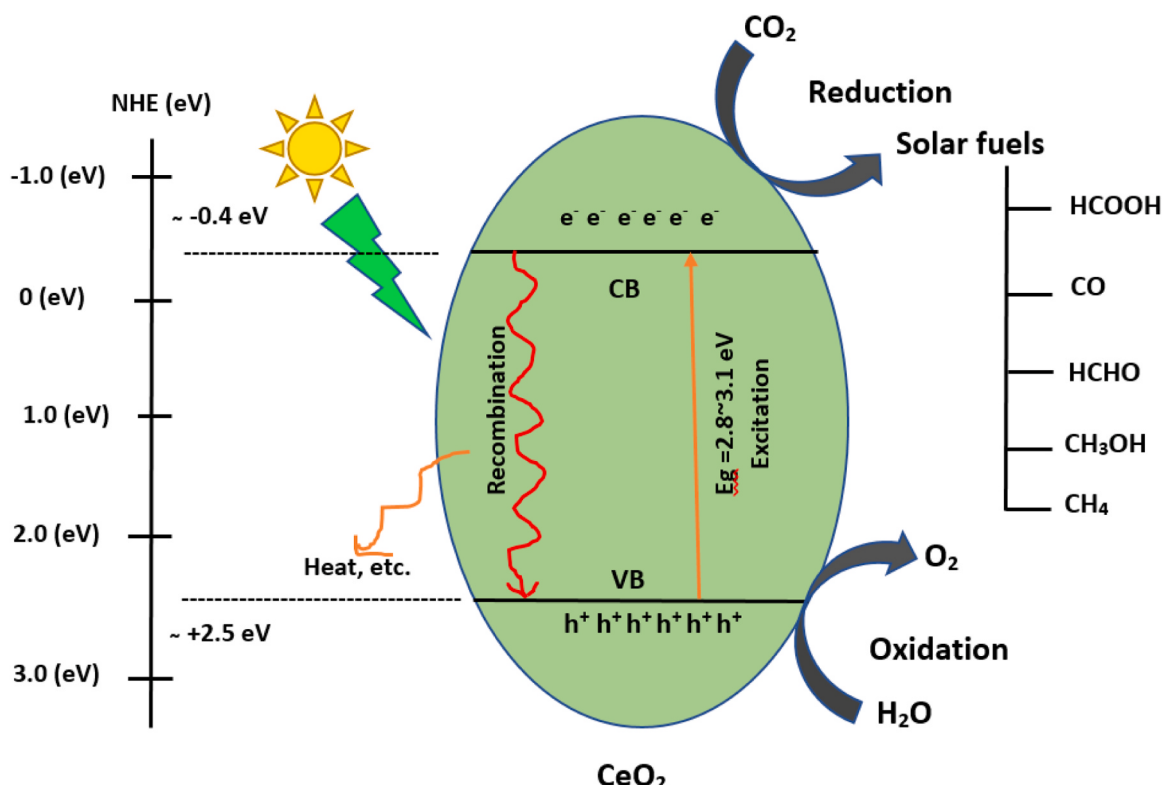


Fig. 1. Proposed photoreduction mechanism of CO_2 into fuels by CeO_2 .

Table 1
Major products of CO_2 reduction and the constant potential ($\text{pH} = 7$).

Reaction	E (V vs NHE)	Product	Reference
$\text{CO}_2 + 2 \text{H}^+ + 2e^- \rightarrow \text{HCOOH}$	-0.61	Formic acid	[57]
$\text{CO}_2 + 2 \text{H}^+ + 2e^- \rightarrow \text{CO} + \text{H}_2\text{O}$	-0.53	Carbon monoxide	[57,58]
$\text{CO}_2 + 4 \text{H}^+ + 4e^- \rightarrow \text{HCHO} + \text{H}_2\text{O}$	-0.48	Formaldehyde	[57–59]
$\text{CO}_2 + 6 \text{H}^+ + 6e^- \rightarrow \text{CH}_3\text{OH} + \text{H}_2\text{O}$	-0.38	Methanol	[57,58]
$\text{CO}_2 + 8 \text{H}^+ + 8e^- \rightarrow \text{CH}_4 + 2 \text{H}_2\text{O}$	-0.24	Methane	[50]
$\text{CO}_2 + 14 \text{H}^+ + 14e^- \rightarrow \text{C}_2\text{H}_6 + 4 \text{H}_2\text{O}$	-0.27	Ethane	[59]

Transition metals, including Fe, Cu, Co, Cr, and Mn, are the most often employed dopants among different elements for optical and photoelectrochemical alteration of semiconductors. Rare earth metal doping and transition metal doping are two categories of metal doping. Impurity energy levels might be introduced into the original bandgap around CB and VB by doping metal ions into CeO_2 . Theoretically, the lattice of CeO_2 would deform if lower valence metals were doped, resulting in oxygen vacancies formation that might operate as CO_2 activation/adsorption sites, reducing CO_2 activation energy/adsorption and promoting photoreduction [61]. One frequent tactic is doping hetero-metal ions (e.g. Mn, Fe, Zr, etc.) to adjust the semiconductors' VB or CB structure. Photocatalytic Reduction CO_2 Conversion of metal and nonmetal doped CeO_2 -based Photocatalysts have been summarized in Table 2.

Wang *et al.* [62] prepared Cr-doped mesoporous CeO_2 photocatalysts using metal nitrates precursors and silica SBA-15 template in a straightforward nanocasting process. The percentage amount of dopant on CeO_2 and its impact on catalytic geometry were investigated in this study. Compared to pristine CeO_2 (2.66 eV), a red shift was obtained

regarding the UV-visible study by adding the dopant amount. The study reported that 20 % of dopant (Cr) can enhance the band gap up to 1.05 eV.

After introducing Cr onto CeO_2 and exposing it to visible light for a more extended period (8 h), the yield of CO and CH_4 increased to $16.2 \mu\text{mol g}^{-1}$ and $10.1 \mu\text{mol g}^{-1}$, respectively, which is two times greater compared to the pristine CeO_2 . The distinct configuration and structure of the mesoporous CeO_2 catalysts doped with Cr, which account for several positive characteristics, are responsible for this exceptional photocatalytic activity. Firstly, a 2D hexagonal porous structure with a large surface area facilitates efficient gas reactant movement to photoactive sites and speeds up product diffusion. Second, adding Cr to mesoporous CeO_2 can significantly increase visible light absorption due to the lowered band gap. Holes and electrons were generated with the catalyst exposed to a longer wavelength. Furthermore, the increased conductivity of Cr-doped CeO_2 would facilitate the separation of photogenerated electron-hole during photocatalysis and interfacial charge transfer, boosting the activity of the process while exposed to visible light (Fig. 2f).

Fe-doped CeO_2 catalysts were produced by Wang *et al.* in 2014 [60] using $\text{Fe}(\text{NO}_3)_3 \cdot 9 \text{H}_2\text{O}$, and their effectiveness as photocatalysts was assessed before the production of Cr-doped CeO_2 . Because the Fe^{3+} ion is smaller than Cr, the Fe-doped catalysts have more significant BET surface areas ($154.2\text{--}176.7 \text{ m}^2 \text{g}^{-1}$) besides pore volumes ($0.368\text{--}0.471 \text{ cm}^3 \text{g}^{-1}$). Mes-FeCe-5, Mes-FeCe-10, Mes-FeCe-20, and Mes-FeCe-30 all showed redshifts in their optical band gap energies compared to Mes- CeO_2 (2.73 eV). After exposure to simulated sunlight for six hours, photocatalytic activity increased with greater Fe doping concentrations, peaking in Mes-FeCe-20 with CO and CH_4 yields of 74.3 and $17.3 \mu\text{mol g}^{-1} \text{ cat.}$, respectively. Yields of CO and CH_4 did not rise further than 20 % Fe doping.

The enhanced efficiency for Fe-doped CeO_2 was attributed to the mesopores in the catalyst's surface and a 2D open-pore arrangement that facilitates reactant diffusion. In addition, the spectral response in longer wavelengths was attributed to adding Fe content that narrowed the band

Table 2Brief of CO₂ reduction by metal and nonmetal doped CeO₂-based photocatalysts.

Mechanism type	Catalyst designation	Synthesis Method name	Reaction Mixtures & Conditions	Reactor type	Light source	Major products with yield	Catalytic stability	References
Metal doping	Zr dopedCeO ₂	co-precipitation method	Catalyst: 20 mg ofCe _{1-x} Zr _x O ₂ catalystReactants:100 mL of 0.016 molL ⁻¹ Na ₂ SO ₃ + CO ₂ Conditions: high-purity CO ₂ gas bubbled at 15 °C.	quartz photoreactor	300-W Xe lamp(white light)	CO(8 μmol g ⁻¹) in 6 hr, CH ₄ (negligible)	High stability(3 cycles)	[64]
	Er-doped CeO ₂ /rGO/CuO	hydrothermal method	Catalyst: photocatalyst of 0.1 gReactants: distilled water 250 mL+NaHCO ₃ (0.1 molL ⁻¹)+ Na ₂ SO ₃ (0.1 molL ⁻¹)Conditions: CO ₂ purged at 298 K	Photoreactor, Type BL-GHX-V	250 W xenonlamp	CH ₄ OH 135.6 μmol g ⁻¹ cat h ⁻¹ in 5 hr	high	[67]
Y, La, and Mo doped CeO ₂	CeY-20	Hydrothermal method	Catalyst:50 mg catalystReactants: CO ₂ +H ₂ O Conditions: CO ₂ gas (99.99 %) bubbled for 30 min at 298 K	glass jar with an optical quartz windowvol. 130 mL	300w Xe arc lamp	CO (ppm) 22 ppm in first 1 hr 8 ppm in first 3 hr NA	4 cycle	[63]
Chromium-doped mesoporous CeO ₂		Nano casting	Catalyst: 0.1 g catalystReactants: 95.5 % CO ₂ + 4.5 % H ₂ OConditions: vacuumed reactor purged with CO ₂ + H ₂ O mixture for 2 h at 30°C, 110 KPa.	homemade stainless-steel reactor	500 W Xenon lamp	CH ₄ (10.1 μmol g ⁻¹) in 8 h. CO (16.2 μmol g ⁻¹)in 8 h.	NA	[62]
Ordered mesoporous Fe-doped CeO ₂		Nano casting (hard template method)	Catalyst: 0.1 g catalystReactants: 95.5 % CO ₂ + 4.5 % H ₂ OConditions: vacuumed reactor purged with CO ₂ + H ₂ O mixture for 2 h at 30°C, 110 KPa.	stainless steel reactor1500 mL	300 W xenon lamp	CH ₄ 17.3 μmol g ⁻¹ in 6 h. CO 74.3 μmol g ⁻¹ in 6 h.	high	[60]
Non-metal doped	S-C/ In ₂ O ₃ -CeO ₂ hollow hexagonal prism	Direct pyrolyzing Ce-doped In-MIL-68 hexagonal prism	Catalyst: 5 mg Reactants: CO ₂ + H ₂ OConditions: CO ₂ gas is purged through deionized water under ambient pressure.	PLS-SXE300, Perfect light photoreactor	Xe lamp (300 W)	CH ₄ 60.6 μmol g ⁻¹ h ⁻¹ CO negligible amount	4 cycles	[71]

gap. Electrons transferred to Fe³⁺ from the forbidden band under solar radiation on Fe-doped catalysts, reducing to Fe²⁺. The photocatalytic function was enhanced by the dissociation of electron-hole pairs produced by photosynthesis. As demonstrated by XPS analysis, Fe³⁺ ion addition increased surface chemisorbed oxygen species, absorbing electrons and producing oxygen radicals with good reduction capacity. A combination of Ce³⁺/Ce⁴⁺ states on the catalyst hindered the mixing of photogenerated electrons and holes, resulting in a higher quantum efficiency for the photocatalytic process.

Li *et al.*, 2018 [64] implemented a valuable and facile co-precipitation method to synthesize hydrangea-like Ce_{1-x}Zr_xO₂ (x = 0.00, 0.025, 0.05 and 0.10). The molar proportion of doped Zr can be changed to control the quantity of oxygen vacancy in the resulting catalytic agent. Various approaches were applied to study the configuration, characteristics, and morphology of the obtained Ce_{1-x}Zr_xO₂. The outcomes of Raman, ESR, and XPS designate that Ce³⁺ formation and O₂ deficiency (10 %) could be enhanced by incorporating Zr as the dopant. The reduction product in the gas phase consisted mainly of CO and trace amounts of CH₄, but no product was found in the liquid medium. The result is influenced by the band gap of Ce_{1-x}Zr_xO₂, which is connected to light harvesting capability. Zr doping narrows the gap due to empty Zr 4d orbital hybridizing with Ce 4 f orbital. Moreover, Zr⁴⁺ is responsible for binding energies of 181.9 and 184.4 eV found in XPS. The improved activity for CO₂ photoreduction seen in the Ce_{1-x}Zr_xO₂ (x = 0.025, 0.05, and 0.10) is explained by the effect mechanism of the oxygen deficiency produced during Zr doping. These findings may help develop a workable strategy to increase photocatalytic activity by revealing the controlled regulation of defects like oxygen vacancies in a photocatalyst. Additionally, doping CeO₂ with rare-earth metals may modify its electronic structure and improve its ability to absorb visible spectra [65,66]. The optical characteristics of rare-earth metal-doped CeO₂ have been extensively studied.

Recently, Wang *et al.* [63] doped three metal ions with CeO₂

nanoparticles using Yttrium nitrate, lanthanum nitrate, and ammonium molybdate as precursors represented as CeM-x, where x denotes the proportion of Ce/M. Among CeM-x, CeM-20 had the greatest CO yields when exposed to Xe-Lamp for five hours. The CeM-20 samples had much better CO₂ photoreduction capabilities than the CeO₂ samples. EPR and XPS analysis indicates that doping with Y and Mo increases the oxygen deficiency amount in CeO₂, which boosts the catalytic activity by facilitating electron and hole transfer and promoting the absorption of UV-visible light. XPS spectra at about 532.5, 531.6, and 529.5 eV are attributed to lattice oxygen in CeO₂ (OL), adsorbed oxygen on surface oxygen vacancies (OV), and chemisorbed oxygen species (i.e. hydroxide) on catalyst surface (OC).

However, Ce and La are lanthanides with comparable atomic radii and valence states. In CeLa-20, the intensity of oxygen vacancy is somewhat reduced. It is possible to see the photoluminescence (PL) spectra of CeO₂ and CeM-20 that are connected to the band-band recombination of the photo-generated charge carriers with the emission photon energy equal to the band-gap. The peaks of these spectra lie at around 560 nm and 460 nm, respectively, and extend to 700 nm. Following the time-resolved fluorescence spectra findings, the peak intensity of CeM-20, particularly CeMo-20, is comparatively lower compared to the pristine CeO₂. This implies that charge separation has been enhanced after doping hetero-metals, and electron-hole recombination has been inhibited. On CeY-20, the CO evolution peaks in the first hour at around 22 ppm, after that drops quickly to 10 ppm, and then declines steadily by 1 ppm h⁻¹. CO₂ adsorption and the intermediary substances produced on the catalyst surface throughout the photoreduction process were thoroughly examined via in-situ FT-IR. Similar carbonates and bicarbonates, such HCO₃⁻, b-CO₃²⁻ and m-CO₃²⁻, are formed on CeO₂ and CeM. It has been shown that the steadily declining CO₂ reduction activity and stability are caused by these intermediates, which have collected and heavily covered on the catalyst surface.

Using a hydrothermal technique, several erbium-doped CeO₂

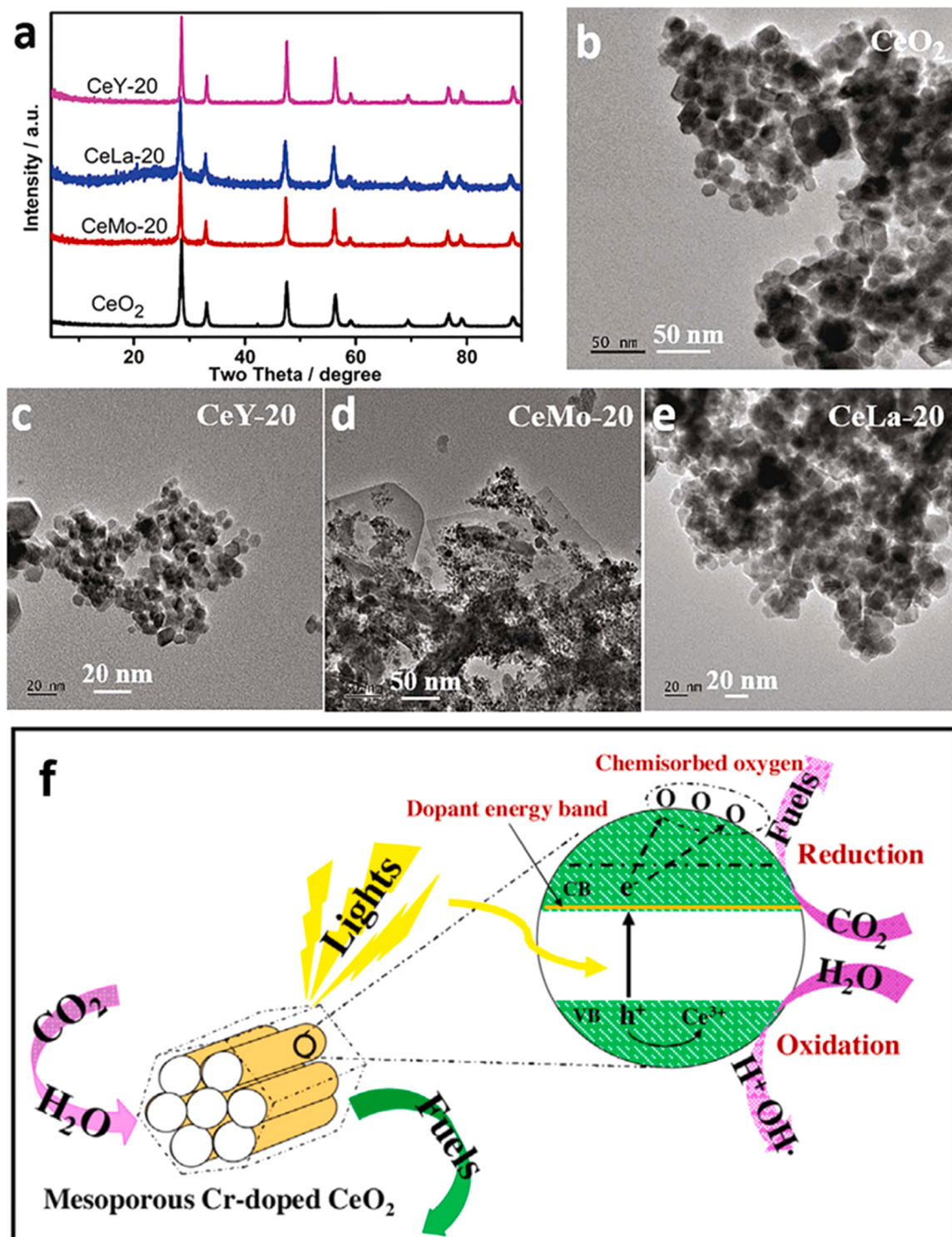


Fig. 2. a) XRD spectra of CeO₂ and CeM-20, b) TEM images of CeO₂ (c) TEM images of CeY-20, (d) TEM images of CeMo-20 (e) TEM images of CeLa-20 [63]. (f) Possible photoreduction mechanism of CO₂ using the Cr-doped mesoporous CeO₂ catalyst [62] Reproduced (adapted) from Copyright 2020 & 2019, Elsevier.

composites loaded with reduced graphene oxide (rGO, referred to as Er-doped CeO₂/rGO) were created [67]. The produced Er-doped CeO₂/rGO composites' crystal structures, morphological traits, and surface physicochemical properties were assessed using XRD, TEM, Raman, UV-visible diffuse reflection, and XPS. By converting CO₂ to methanol, the composite samples' photocatalytic activity was assessed in further detail. The findings demonstrate that rGO loading shifted the response spectrum to 467.9 nm and that erbium (III) doping redshifted

the response spectra from 392 nm to 451 nm. Under the same conditions, the corresponding CO₂ to methanol reduction yields for Er-doped CeO₂/CuO and Er-doped CeO₂/rGO/CuO catalysts approached 42.5 and 135.6 μmol g⁻¹h⁻¹, respectively. Among all the metal-doped CeO₂, CO₂ reduction efficiency of Er-doped CeO₂/CuO and Er-doped CeO₂/rGO/CuO catalysts to produce methanol was greater (42.5 and 135.6 μmol g⁻¹h⁻¹ in 5 hr, respectively). For the CeO₂, Er-doped CeO₂, and Er-doped CeO₂/rGO samples, the calculated direct band gaps were

2.65 eV, 2.75 eV, and 3.15 eV, respectively. Doping of CeO₂ with erbium (III) ions results in greater oxygen vacancies and a smaller band gap.

A semiconductor's inadequate thermodynamic performance might result from doping metal ions. Metal ions have the potential to readily form recombination centers in semiconductors, which would hinder the separation of e⁻ h⁺ couples and result in poor thermodynamic strength of the photocatalyst [68,69]. As a result, doping CeO₂ with nonmetal ions has garnered much interest. Nonmetal ion doping in a catalyst often forms a new VB on top of the existing one. The absorption zone of TiO₂ displayed a red-shift to visible light after the doping with nonmetal elements (N, C, F, S, etc.). The occurrence may be explained by hybridizing the nonmetal element's p orbital with O 2p, which shifted the VB edge northward and lowered the prohibited band [70]. Consequently, it is possible to deduce that the density of states close to CeO₂'s VB edge may alter if N is doped.

Qi Wang *et al.* synthesized [71] a newly developed sulfur-doped photocatalyst with a thin carbon coating (S-C/ In₂O₃-CeO₂ HHP) by pyrolyzing Ce-doped In-Materials of Institute Lavoisier-68 (In-MIL-68) hexagonal prism metal-organic structure directly under N₂ atmosphere in the presence of sulfur powder, showing excellent photocatalytic carbon dioxide (CO₂) reduction efficiency. This synthetic approach enabled control of the final product's structure and surface defects. The hollow porous hexagonal prisms' numerous reflections offer more active sites, excellent light usage, and quick mass transfer of reactants and products. These benefits can be further enhanced in the interim by surface imperfections associated with oxygen vacancies. The band gap may be lowered by sulfur doping and carbon coating because combining O and S 2p orbitals produces more intermediate electronic states. S-C/ In₂O₃-CeO₂ HHP exhibited greater photocatalytic activity for CO₂ reduction to CH₄ (60.6 μmol g⁻¹h⁻¹) with 92.4 % selectivity and CO under AM1.5 irradiations.

2.2. Oxygen Vacancies

It is preferable to generate oxygen vacancies as self-doping without the addition of any extra contaminants, as this might increase CeO₂'s photocatalytic activity without jeopardizing its inherent crystal structure [72]. CeO₂ can be synthesized by several physical and chemical approaches [73]. Still, the most commonly employed techniques need much time and/or energy. Moreover, calcination (another energy-intensive process) is typically used to self-dope CeO₂ by generating oxygen vacancies [72]. A summary of photocatalytic reduction CO₂ conversion by a generation of oxygen vacancy on CeO₂-based photocatalysts have been summarized in Table 3.

Hezam *et al.* [74] modified the solution combustion synthesis (SCS)

method and developed a new process called sunlight-assisted combustion (SAC), which uses sustainable energy from the sun to initiate a combustion reaction among C₂H₅NO₂ and Ce-(NO₃)₃·6 H₂O and introduces oxygen vacancies in CeO₂. The whole reaction was executed in a double-necked flask semi-closed system, eliminating pollution concerns and providing a sustainable and environmentally friendly technique for synthesizing nanoparticles. Fig. 3e shows the schematic design for the configuration. In contrast to the conventional solution combustion (CSC) method, along with causing oxygen vacancies in CeO₂, solar light begins uniform preheating, developing more homogeneous and smaller CeO₂ nanoparticles. This improves charge carrier separation effectiveness, photocatalytic activity, and light absorption. Sunlight is utilized as a fresh, renewable energy supply to achieve consistent pre-heating, start the exothermic combustion event, and lead to surface oxygen vacancies. Uniform tiny nanoparticles were developed due to the SAC process's uniform heating. The oxygen vacancies that were produced caused CeO₂'s band gap to shrink, light absorption to rise, and CO₂ capture efficiency to increase. Fig. 3a, b compares the fitted Ce 3d XPS spectra of the two samples to determine the Ce states. In CeO₂-CSC, the binding energies of Ce⁴⁺ 3d^{5/2} and 3d^{3/2} peaks appear at 898.89 and 917.05 eV, respectively, while the Ce³⁺ 3d^{5/2} and Ce³⁺ 3d^{3/2} peaks are located at 902.13 and 883.03 eV, respectively. The ratio of lattice oxygen vacancy (OL) to total oxygen vacancy (OT) is 0.62 and 0.38 for CeO₂-CSC and CeO₂-SAC, respectively (Fig. 3c, d). Hence, the photocatalytic CO₂ reduction efficiency to CH₃OH of CeO₂ synthesized through the SAC process was greater (0.702 μmol g⁻¹h⁻¹) than that of the CSC (0.397 μmol g⁻¹h⁻¹) process.

The impact of the oxygen vacancy brought on CeO₂ for CO₂ reduction has been explored briefly by M. Wang *et al.* in 2019 [75], Cu has been added to stabilize and produce O deficiency in CeO₂, resulting in significantly improved catalytic activity for CO₂ photoreduction within the UV-Visible range. Oxygen vacancy also increases the electron-hole transfer, extends the carriers lifetime, provides more active sites, and modifies the configurations of CeO_{2-x}. Two different oxidation states (Ce³⁺ and Ce⁴⁺) are generated in the Cu/CeO_{2-x} where Cu exists as Cu⁰, concomitant with Cu's entry and oxygen vacancy formation. As per the XPS and Raman spectra, it has been confirmed that introduced Cu helps chemicals stabilize O vacancies, which results in increased and sustained photocatalytic activity. The sample Cu/CeO_{2-x-0.1} exhibits the maximum photocatalytic activity with a CO yield of about 8.25 μmol g⁻¹ after 5 h of Xe-light radiation, which is almost 26 times greater than that on CeO_{2-x}. Trace CH₄ was also noticed.

M. Wang *et al.* [76] considered CeO₂ as a n-type semiconductor with the advantages of nontoxicity, increased stability against photo-corrosion, and so on. They chose this photocatalyst to introduce oxygen vacancy on its surface by the Oxalic acid-N₂ method. The oxygen

Table 3
Brief of CO₂ reduction on CeO₂-based photocatalysts by oxygen vacancy generation.

Mechanism type	Catalyst designation	Synthesis Method	Reaction Mixtures & Conditions	Reactor type	Light source	Major products with yield	Catalytic stability	References
Oxygen Vacancy	CeO ₂ -SAC	Sunlight-assisted combustion Synthesis	Catalyst: 50 mg of photocatalyst Reactants: 10 mL of ultrapure deionized water + 0.12 g of NaHCO ₃ + CO ₂ Conditions: purged with argon for 30 min	135 mL quartz reactor	300 W Xe lamp	CH ₃ OH (0.702 μmol h ⁻¹ g ⁻¹)	3 cycles	[74]
	Cu/CeO _{2-x-0.1}	hydrothermal method	Catalyst: 50 mg of photocatalyst Reactants: CO ₂ Conditions: CO ₂ purged for 30 min at 298 K	500 mL glass reactor with an optical quartz window	300 W Xe-arc lamp	CO 8.25 μmol g ⁻¹ in 5 h	3 cycles	[75]
	Surface modified CeO ₂ by OA-N ₂	hydrothermal method	Catalyst: 50 mg of photocatalyst Reactants: CO ₂ Conditions: CO ₂ purged for 30 min at 298 K	130 mL glass jar with an optical quartz window	300 W Xe-arc lamp	CO 12.35 ppm in 5 h	3 cycles	[76]

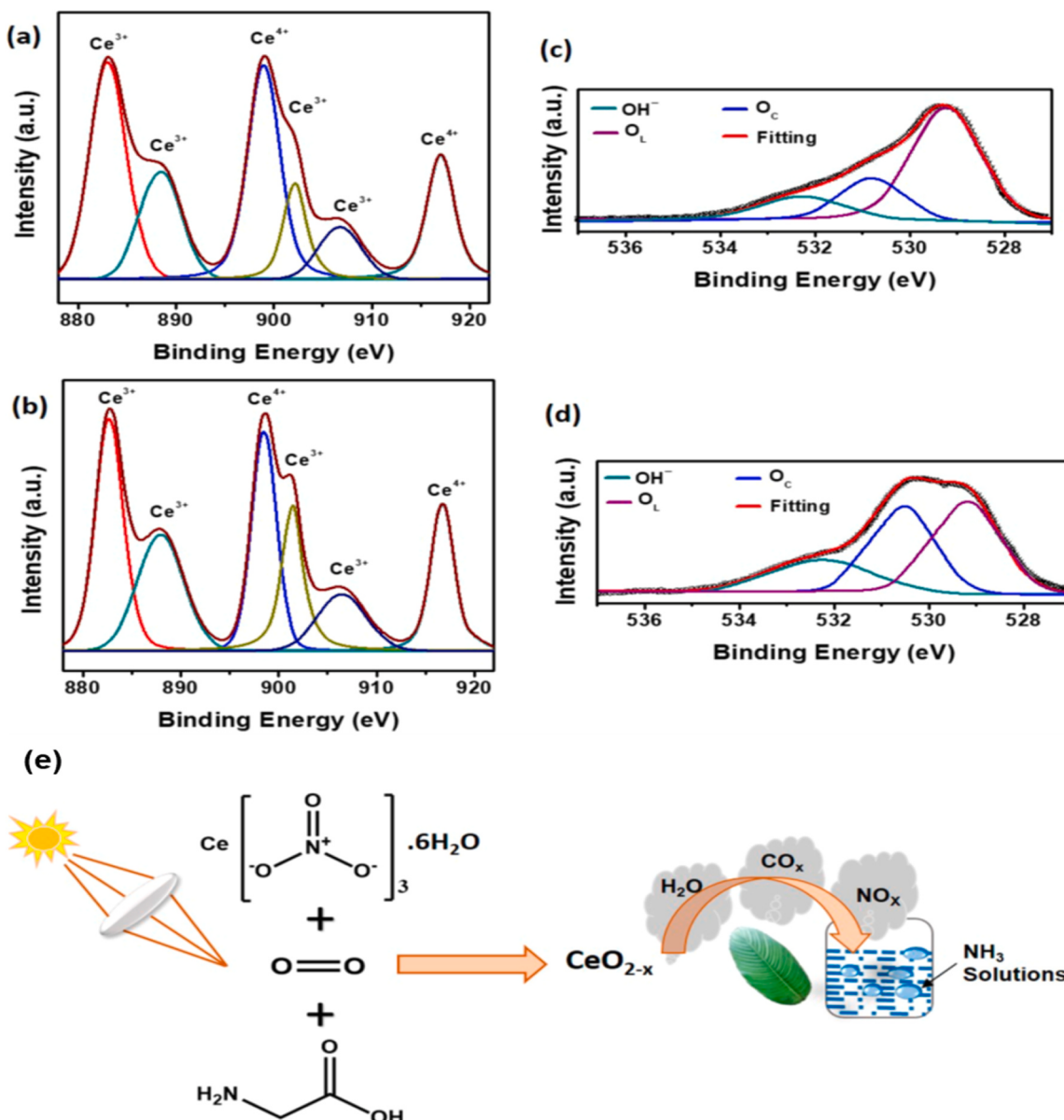


Fig. 3. Ce 3d XPS spectrum of (a) CeO₂-CSC, (b) CeO₂-SAC, O 1 s XPS spectrum of (c) CeO₂-CSC, and (d) CeO₂-SAC, and (e) Sunlight-driven combustion synthesis of CeO₂ with improved oxygen vacancies (CeO_{2-x}). Reproduced (adapted) from [75]. Copyright 2020, ACS.

vacancy-enriched CeO₂ has minimally altered the band structure of CeO₂, but it has boosted the unpaired electrons and prolonged the lifespan of photo-generated carriers. This treatment has resulted in a much higher ratio of Ce³⁺/Ce⁴⁺ in CeO₂. CO is the main reduction product and yields around eight times higher than pure CeO₂, demonstrating noticeably increased photocatalytic activity in CO₂ reduction. The abundant oxygen vacancy greatly boosted the CO₂ adsorption/activation on the surface of CeO₂, as demonstrated by in-situ FT-IR spectra.

Nonetheless, the primary hindrance to preserving the elevated stability of CeO₂ and CO₂ reduction efficiency with O vacancy may be the carbonates that are firmly adsorbed on the photocatalyst surface. This work suggests a possible path toward synthesizing and optimizing semiconductor photocatalysts with sustainably boosted reduction capacity of CeO₂. It also initiates a new approach for creating oxygen vacancies on the surface of metal oxides and exposes the potential roles of oxygen vacancies in enhancing the CO₂ photoreduction activity of CeO₂.

2.3. Nanocomposites

2.3.1. Clay-supported CeO₂

CeO₂ is a well-known semiconductor material that has been effectively manufactured in a variety of ways and includes forms cube, rod-like, and nanoparticle forms [77–80]. There are a few inadequacies for the stated CeO₂ to be sufficiently focused: (i) readily recombine photo-generated carriers; (ii) minimal light energy consumption; and (iii) stack and agglomerate of CeO₂. Making structural or composite modifications for pure CeO₂ is one workable method. To increase the active sites and avoid CeO₂ aggregation, ATP may be of assistance. However, electrons carried by ATP can encourage the splitting of the pair of electrons and holes, which may assist the catalytic activity. It is worth to mention there haven't been many reports of CeO₂ modification using ATP for photocatalytic C-FC.

With this continuation, Jia Zheng *et al.* [81] fabricated modified CeO₂ (CeO₂/ATP) by facile synthesis method. The optimal CeO₂/ATP photocatalyst product revealed a higher conversion rate of CO₂ into CO and CH₄. Moreover, the product showed an improved surface area of

$101.4 \text{ m}^2\text{g}^{-1}$. More accessible active sites might result from the enhanced surface area, improving their ability to reduce CO_2 emissions. The mesoporous framework and pores of CeO_2 were boosted by the addition of ATP, which enables CeO_2/ATP to reduce CO_2 . The photo-generated electrons can move to the CB of CeO_2 in the presence of light. Hence, at the CB of CeO_2 , photoinduced electrons (e^-) accumulate and convert CO_2 to CO and CH_4 . CO_2 to CO has a reduction potential of -0.53 eV , whereas CO_2 to CH_4 has a potential of -0.24 eV . There is enough driving force to support CO_2 photoreduction since the energy of the CB for CeO_2/ATP can match the energy needed to reduce CO_2 to CH_4 and CO.

According to Viktoria *et al.* [82] in the presence of visible and infrared light, the photothermal effect might enhance the catalytic activity of the methanation process because of the localized surface plasmonic characteristics of the Ni nanoparticles in the Ni/CeO_2 catalyst. The SBA-15 templates were impregnated with cerium and nickel nitrates and then annealed to produce the Ni/CeO_2 catalyst. To achieve an expected 15 % Ni by mass in the finished product, the Ni/Ce ratio was used. They reduced the power usage by 20 % compared to dark conditions because the high surface area catalyst developed shows a 2.4-fold improvement in the reaction rate under solar radiation. Both in-situ DRIFT spectrometry and light-assisted CO_2 conversion studies, conducted at varying illumination intensities, have demonstrated a twofold influence of incoming photons on the catalytic characteristics of the two-component Ni/CeO_2 photocatalyst. Ni nanoparticles are affected by causing a localized surface plasmon resonance, which is then followed by heat dissipation into the oxide matrix.

Mesoporous cerium oxide ($m\text{-CeO}_2$) was prepared successfully by Haopeng Jiang *et al.* [83] using a porous SBA-15 (specific surface area $150.79 \text{ m}^2\text{g}^{-1}$) molecular sieve as a template. Then, the hydrothermal technique was applied to modify $m\text{-CeO}_2$ photocatalysts by g-C₃N₄ quantum dots (CN QDs). TEM, HRTEM, and XPS demonstrated that CN QDs are effectively loaded on the $m\text{-CeO}_2$ surface. Simultaneously, the effect of varying CN QDs on CeO_2 catalytic activity was studied. The preparation of the 0.75CN QDs/ $m\text{-CeO}_2$ composite photocatalyst for CO and CH_4 yields 2.83 times ($22.48 \mu\text{mol g}^{-1}$) and 7.71 times ($15.81 \mu\text{mol g}^{-1}$) as monomer $m\text{-CeO}_2$, respectively, according to the experimental findings, which demonstrate the composite photocatalyst's strong ability to convert CO_2 as photocatalyst. The Ce 3d and O 1 s peaks in 0.75 wt percent CN QDs/ $m\text{-CeO}_2$ show a little shift towards high binding energy when the CN QDs are changed on $m\text{-CeO}_2$, indicating a strong interaction between CN QDs and $m\text{-CeO}_2$. The CN QDs function as an electron excitation center and transport receptor in this reduction system. In addition to functioning as dots-like semiconductors, the CN QDs take charge of excitation and transfer. More charge transfer channels may be built using CeO_2 after loading CN QDs, compared to the previous loading of CN QDs. This is achieved by conducting a large number of tiny heterojunctions. When $m\text{-CeO}_2$ is exposed to UV light, holes are produced in the valence band location, and the conduction band can stimulate electrons in the valence band. Triethanolamine (TEOA) can reduce the likelihood of photogenerated electron-hole recombination. Some of the electrons produced by $m\text{-CeO}_2$ are involved in the CO_2 reduction reaction, while other electrons are transferred to CN QDs across the two-phase interface to participate in the CO_2 catalytic reaction.

2.3.2. CeO_2 with Co-catalysts

Photocatalysis uses catalysts to boost catalytic activity due to their fast kinetics and low overpotential. They increased photocatalytic activities in both reduction and oxidization by increasing the separation efficiency of photo-generated electron-hole pairs via p-n heterojunction upon irradiation, adsorbed target molecules, and reduced recombination by capturing photogenerated electrons or holes. They used surface plasma to expand the incident irradiation spectrum's absorption range. According to S. Zhou and S. Liu's 2017 [84] study ING/CeO_2 hybrid material was developed by dispersing CeO_2 on ING sheets. The hybrid material was then characterized using XRD, TEM, Raman, UV-visible

diffuse reflectance, and surface photovoltaic spectroscopy. ING/CeO_2 hybrid material adsorbed Cu(II) ions, which capture photogenerated electrons and convert CO_2 to methanol when exposed to light. To determine Cu(II) function, XPS measurements were taken before and after photocatalysis. The photocatalytic energy shifting of $\text{Cu} 2p^{3/2}$ and $\text{Cu} 2p^{1/2}$ by 0.7 eV showed the emergence of the Cu(I) intermediate. The photoreduction process of CO_2 to CH_3OH was postulated, considering ING and Cu(II) effects and Cu(I) intermediate preparation. First, Cu(II) attracted photo-generated electrons, then reduced to Cu(I). Cu(I) interacts quickly with CO_2 to form CH_3OH in numerous steps and returns to Cu(II) simultaneously. For Cu(II)/ING/ CeO_2 , $385.8 \mu\text{mol g}^{-1}\text{h}^{-1}$ CH_3OH was produced, whereas ING/ CeO_2 produced just 3.57. CO_2 photocatalytic reduction benefits from Cu(II) ions. ING/ CeO_2 hybrid material showed increased photocatalytic CO_2 reduction through Cu(II) ions and ING sheets, with 3.6 % of ING reaching optimum CH_3OH yield.

2.3.3. Coupling CeO_2 with other Semiconductor nanomaterials

Studying and developing new materials and technologies that can capture CO_2 and transform it into valuable chemicals or goods is essential to ensure a sustainable energy future. Activating steady CO_2 is the main obstacle, though. To achieve CeO_2 's more effective photoactivity, heterostructures made by combining it with two or more nanomaterials are thought to be very promising. The enhancement of photoreduction behaviors resulted from the synergistic effects of several nanomaterials, which led to superior stability, better use of visible light, and efficient charge separation and relocation [85,86].

2.3.3.1. Binary/ ternary hybrid heterostructures. Regarding binary CeO_2 -based composites, it makes sense to modify CeO_2 by mixing it with other appropriate semiconductors. To elucidate the increased visible-light-induced photocatalytic activity of CeO_2 -based composites, four potential charge transfer channels are often considered, e.g., the conventional type II, p-n junction, and Z-scheme, as shown in Fig. 4.

2.3.3.2. Type II Mechanism. CeO_2 is generally paired with larger band-gap nanomaterials as a light-absorbing medium or enhanced with additional semiconductors with low energy gaps in type II heterojunctions. Even if the exact mechanism is unclear, the simplified explanation of CO_2 photoreduction below (Fig. 4A) is understandable. Visible light excites a semiconductor, producing photogenerated electron-hole pairs that control redox reactions. Visible light excited the electrons of SC1, transporting them from VB to CB and leaving holes at VB. After stimulating CeO_2 's CB, the electrons also left holes at VB. Water molecules were oxidized to h^+ , e^- , and O_2 . Meanwhile, the remaining holes at the CeO_2 VB traveled to the SC1 VB. CeO_2 showed a greater rate of electron-hole pair recombination than SC1. However, the SC1- CeO_2 heterojunction had the lowest recombination, indicating successful separation and leading to the highest photoactivity. The excited electrons at the CB of SC1 easily move to the lower energy CB of CeO_2 . In this example, the photoreduction process was substantially influenced by the Ce^{4+} and Ce^{3+} oxidation states. Excited electrons at CeO_2 's CB decrease Ce^{4+} to Ce^{3+} , effectively accepting electrons from SC1. When Ce^{3+} of CeO_2 comes into contact with CO_2 , it is converted into Ce^{4+} and CO_2 , which is subsequently reduced to CH_3OH , CO, and other fuels using h^+ and e^- resulting from water molecule oxidation. Ce^{4+} was again transformed into Ce^{3+} to accept electrons in visible wavelengths.

Herein, we reviewed CeO_2 coupled with different semiconductors for the reduction of CO_2 in various solar fuels following the Type II mechanism (Table 4). Qingping *et al.* [49] applied the solvothermal method to synthesize high surface mesoporous CeO_2 (bandgap 2.17 eV) supported CdS (bandgap 2.57 eV) nanocomposite CdS@CeO_2 (band gap of 2.13 eV) which confirmed the maximum production of $1534 \mu\text{mol g}^{-1}$ methanol and $213 \mu\text{mol g}^{-1}$ CO in 10 hrs under analogous conditions. On the other hand, Sana Ijaz *et al.* [87] applied a two-step

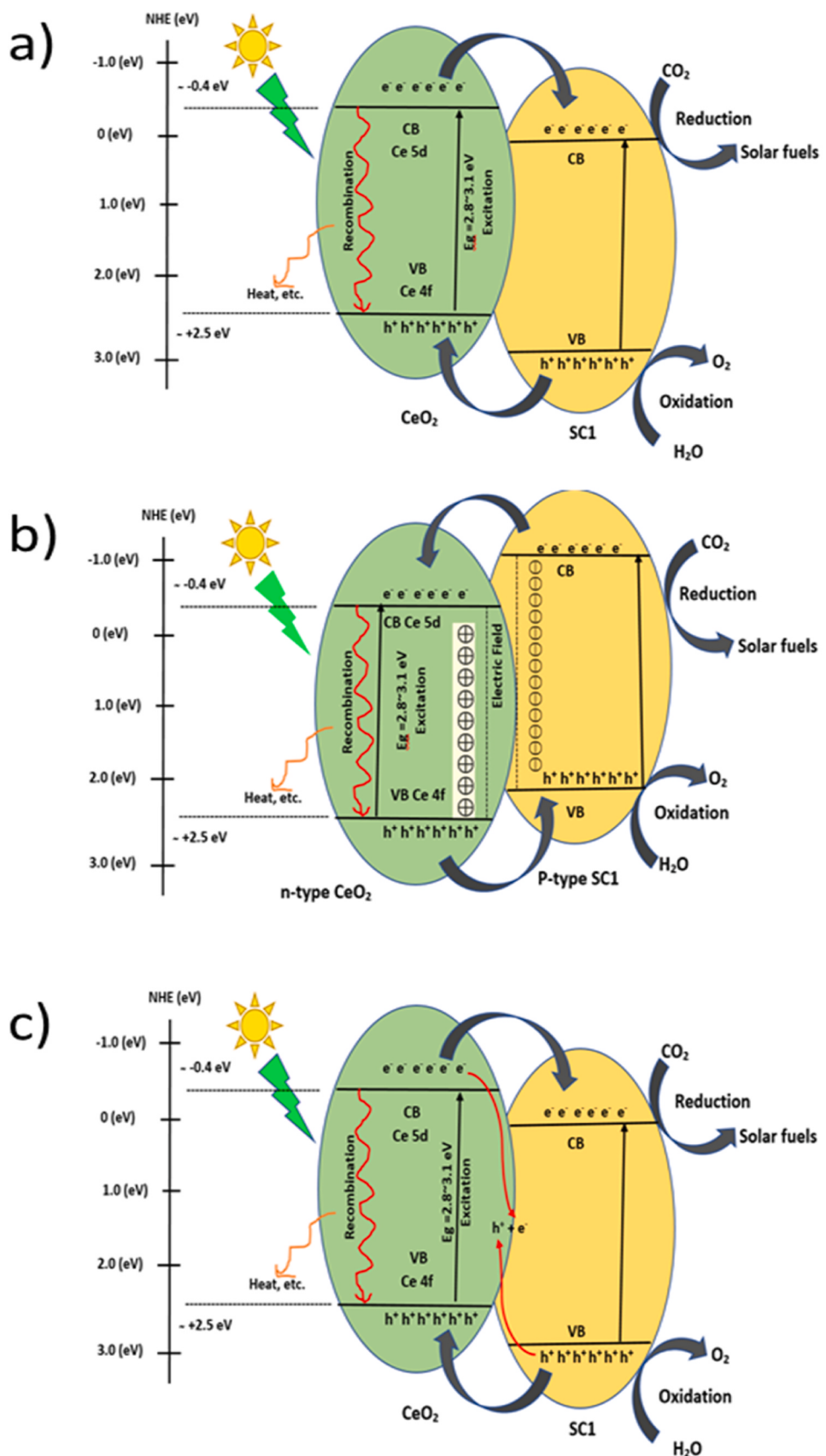


Fig. 4. Proposed photoreduction mechanisms a) Type II: hybridize with SC1; b) p-n heterojunction system, c) Z-Scheme.

Table 4Summary of photocatalytic reduction of CO₂ conversion of CeO₂-based nanocomposite Photocatalysts.

Mechanism type	Catalyst designation	Synthesis Method	Reaction Mixtures & Conditions	Reactor type	Light source	Major products with yield	Catalytic stability	References
	CeO ₂	hydrothermal method	DMF, TEA and water in a 2:2:1 ratio, 50 mg of CeO ₂ , N ₂ gas	Quartz photoreactor	300 W Xe lamp	CH ₃ OH (267 μmol g ⁻¹) CO (29 μmol g ⁻¹) in 10 h.	NA	[49]
Clay supported	CeO ₂ /ATP-1 wt%	high temperature calcination	Catalyst: 0.05 g photocatalystReactants: CO ₂ + NaOH + acetonitrileConditions: CO ₂ passed through for 30 min	quartz reactor	UV light (254 nm, 8 W).	CO 309.44 μmol g ⁻¹ h ⁻¹ CH ₄ 184.33 μmol g ⁻¹ h ⁻¹	NA	[81]
	Ni/mesoporous-CeO ₂ (SBA-15 template)	Impregnation method	Catalyst: 0.05 g photocatalystReactants: CO ₂ + NaOH + acetonitrileConditions: (80 % H ₂ + 20 % CO ₂) gas flow at 20 mL min ⁻¹ rate of	A custom-made flow-type gas reactor	300 W solar simulator (Xelamp)	CH ₄ 2.6 μmol g ⁻¹ min ⁻¹	NA	[82]
	g-C ₃ N ₄ quantum dot/mesoporous- CeO ₂	Hydrothermal method	Catalyst: 0.1 g photocatalystReactants: CO ₂ + NaOH + TEOAConditions: pressure 0.4 MPa	Photoreactor	8 W UV-light lamp.	CO 22.48 μmol g ⁻¹ in 10 hrs CH ₄ 15.81 μmol g ⁻¹ in 10 hrs	8 cycles	[83]
CeO ₂ with Co-catalysts	N-dopedgraphene/ CeO ₂ Cu(II) as co-catalyst	Hummers method	Catalyst: 0.1gReactants: CO ₂ + H ₂ O + NaHCO ₃ + Na ₂ SO ₃ Conditions: Initial pH= 6.8, Temp = 298 K, Time = 8 hrs	Photoreactor (Type BL-GHX-V).	250 W Xe lamp.	CH ₃ OH 385.8 μmol g ⁻¹ h ⁻¹	NA	[84]
Type II Heterojunction	CdS@ CeO ₂	two-step chemical method	Catalyst: 10 mgReactants: CO ₂ + H ₂ OConditions: Pressure=25 kPa, Temp=150°C, Time= 8 hrs	Quartz reactor	300 W Xe lamp	CH ₄ 7.00 μmol g ⁻¹ in 8hr 1000 μmol g ⁻¹ CH ₃ OH in 8 hr	Photocatalytically stable	[87]
	CdS/mesoporous CeO ₂	Solvothermal process	Catalyst: 50 mgSolvents: DMF, TEA, and water in a 2:2:1 ratio,Reactants: CO ₂ + H ₂ OGas: N ₂ gas	quartz reactor	300 W Xe lamp	CH ₃ OH1534 μmol g ⁻¹ in 10 hr CO 213 μmol g ⁻¹ in 10 hr	6 cycles	[49]
	3 %mesoporous CeO ₂ /g-C ₃ N ₄	hard-template route	Catalyst: 50 mgReactants: CO ₂ + H ₂ OTemp.= 25C (after 2nd and 3rd run temperature-150C)	gas-closed circulation system reactor	300 W Xe-arc lamp	CH ₄ 0.694 μmol h ⁻¹ CO 0.508 μmol h ⁻¹	4 cycles	[88]
	g-C ₃ N ₄ /Ag/ CeO ₂ -mesoporous	nanocasting pathway	Catalyst: 0.1 g photocatalyst, Reactants: CO ₂ + NaOH (0.1 M)Sacrificial agent: triethanolamine (TEOA)Conditions: 0.4 MPa pressure and room temperature	closed photochemical reactor	8 W UV-light lamp	CO 13.94 μmol g ⁻¹ in 10hrs CH ₄ 7.39 μmol g ⁻¹ in 10 hrs	5 cycles	[89]
	3 mL HAuCl ₄ .4 H ₂ O containing C ₃ N ₄ / Au/ CeO ₂ /Fe ₃ O ₄ (3-CACeF)	Hydrothermal calcination, deposits grow and self-assembly	Catalyst: 0.1 g,Reactants: 250 mL NaHCO ₃ (0.1 mol L ⁻¹) + 0.1 mol L ⁻¹ Na ₂ SO ₃ ,CO ₂ Purging: 20 minpH 6.8, 4 hr	Photoreactor (Type BL-GHX-V).	250 W Xe lamp.	CO 28 μmol g ⁻¹ after 4 hr CH ₄ 9.5 μmol g ⁻¹ after 4 hr	4 cycles	[90]
	10In/Ce/HCl treated ATP-20	one-step method	Catalyst: 0.1 g photocatalystReactants: 100 mL NaOH (0.1 M) + triethanolamine (TEOA) in reactor, CO ₂ ,Conditions: CO ₂ gas bubbled for 30 min	Closed photochemical reactor	8 W UV-light lamp	32.03 μmol g ⁻¹ CO in 6hrs 16.94 μmol g ⁻¹ CH ₄ in 6hrs	4 cycles	[93]
	ZnO/ CeO ₂ molar ratio-1	Flame-spray pyrolysis (FSP)	Catalyst: 20 mg photocatalyst.Reactants: ultra-pure CO ₂ (99.999 %) + 10 mL of deionized waterPressure: 71 kPaTemp.: 20C	Pyrex glass reactor	300 W Xe lamp	0.526 μmol g ⁻¹ h ⁻¹ CO 0.069 CH ₄ μmol g ⁻¹ h ⁻¹	1 cycle	[94]
	CeO ₂ /Bi ₂ MoO ₆ (wt ratio 5:1)	Solvothermal	Catalyst: 0.05 g photocatalystReactants: 50 mL ultrapurewater+ CO ₂ gasBubbled, 30 minConditions: 4C	quartz glass reactor	300 W Xe arc lamp	CH ₃ OH 32.5 μmol g ⁻¹ h ⁻¹ C ₂ H ₅ OH 25.9 μmol g ⁻¹ h ⁻¹	4 cycles	[92]
	modified TiO ₂ /rGO/ CeO ₂ composite	Ultrasonically-assisted surface-modified method	Catalyst: 0.15 g of photocatalystsReactants: CO ₂ + H ₂ OConditions: CO ₂ purging for 30 min at 0.025 Lmin ⁻¹ at arte	photoreactor	15 W UV-C (254 nm) HgLamp	CH ₃ OH 641 μmol g ⁻¹ h ⁻¹ C ₂ H ₅ OH 271 μmol g ⁻¹ h ⁻¹	NA	[95]

(continued on next page)

Table 4 (continued)

Mechanism type	Catalyst designation	Synthesis Method	Reaction Mixtures & Conditions	Reactor type	Light source	Major products with yield	Catalytic stability	References
p-n junction	Fe-Ni@ CeO ₂ Nano rods (FNC)	template-assisted decoration	Catalyst: 50 mg photocatalystReactants: 10 mL TEA, 30 mL DMF, and 10 mL water, CO ₂ .Conditions: N ₂ gas bubbling for 10 min to evacuate air.CO ₂ purging, 30 min	60 mL cylindrical vessel.	20 W white LED light ($\lambda > 400$ nm).	7039 $\mu\text{mol g}^{-1} \text{ h}^{-1}$ CH ₃ OH in 24 hr	5 cycles	[96]
	Flower-like CeO ₂ /CuO	Electrodeposition	CeO ₂ NPs/CuO NPs composite catalyst as the working electrode, temperature of 25 °C, aqueous 0.1 mol L ⁻¹ KHCO ₃ (40 mL), CO ₂ gas	Photo Electrochemical cell	Visible light (500 W Xe Lamp)	3.44 $\mu\text{mol cm}^{-2} \text{ h}^{-1}$ - CH ₃ OH		[97]
	15 % Bi ₂ O ₃ /CeO ₂	Sol-gel	Catalyst: 2.8 g L ⁻¹ Reactants: 125 mL of H ₂ O+ heated to 80 °C+ 135 mg of Na ₂ CO ₃ + 0.315 mL of 4 M HCl	Homemade Photoreactor	300 W Xe lamp	CH ₃ OH 1300 $\mu\text{mol g}^{-1}$ after 9 h of	5 cycles	[98]
Z-Scheme	NiFeCr-LDH-(PCN/ CeO ₂)LDHs= hierarchical flower-like ternary layered double hydroxidesPCN=polymeric carbon nitride	hydrothermal method	Catalyst: 50 mg Photocatalyst.Reactants: CO ₂ + H ₂ O, 2mLTEOA/CH ₃ CN/H ₂ O = 1:3:1 (v/v/v)[TEOA=triethanolamine, DMF=Dimethylformamide]Conditions: 0.2 MPa pressure	quartz round dish	300 W Xe light	CO 52.1 $\mu\text{mol g}^{-1} \text{ h}^{-1}$, CH ₄ 17 $\mu\text{mol g}^{-1} \text{ h}^{-1}$,	7 cycles	[99]
	Cu ₂ O/WO ₃ / CeO ₂	hydrothermal method	Catalyst: 50 mg photocatalystReactants: DMF/H ₂ O/TEA (3:1:1) + CO ₂ .Conditions: N ₂ purging for 30 min[TEA=trimethylamine]	borosilicate glass	20 W white LED	CH ₃ OH 3182 $\mu\text{mol g}^{-1} \text{ h}^{-1}$	5 cycles	[100]
	(Cs ₃ Bi ₂ I ₉ / CeO ₂ -nanosheets3:1)	self-template-orientedmethod	Catalyst: required amount of PhotocatalystReactants: CO ₂ + H ₂ O	gas-solid reactor,	300 W Xe lamp	CH ₄ and COTotal yield 877.04 $\mu\text{mol g}^{-1}$	3 cycles	[101]
	SnS ₂ / CeO ₂ (40 %)	Hydrothermal	Catalyst:Reactants: CO ₂ + H ₂ O/TEOA as sacrificial agent	Liquid phase system	300 W Xelamp	CO yields of 9.35 $\mu\text{mol g}^{-1} \text{ h}^{-1}$ CH ₄ 9.35 $\mu\text{mol g}^{-1} \text{ h}^{-1}$	3 cycles	[102]
	Phosphate decorated-octahedral CeO ₂ / g-C ₃ N ₄	Hydrothermal Method	Catalyst= 50 mg photocatalyst.Reactants: H ₂ O + CO ₂ Conditions: 4 bar CO ₂	Teflon-lined autoclave	300 W Xe lamp	CO 4.184 $\mu\text{mol g}^{-1}$	3 cycle	[103]
S-scheme	3D flower-like Ag-ZnO-CeO ₂ (AgCZ)	hydrothermal–photodeposition	Catalyst: 50 mg of the photocatalyst, Reactants: CO ₂ + DI water,Conditions: sonicated for 30 min, 80 °C in a hot air oven,	quartz reactor	sunlight irradiation	CO~377.75 $\mu\text{mol g}^{-1} \text{ h}^{-1}$ CH ₄ ~20.12 $\mu\text{mol g}^{-1} \text{ h}^{-1}$	5 cycles	[104]
	rGO/Rod like-CeO ₂ /g-C ₃ N ₄	Hydrothermal process	Catalyst: Required amountReactants: CO ₂ , H ₂ O	NA	Xe-lamp (300 W)	CO 63.18 in 4 h CH ₄ 32.67 $\mu\text{mol g}^{-1}$ in 4hrs	4 cycles	[105]

chemical process to synthesize CdS@CeO₂ composite with previously prepared pure fluorite cubic structured CeO₂ and cubic CdS microspheres nanoparticles through a hydrothermal synthesis approach for the photocatalytic reduction of CO₂ with water under visible light illumination. CH₄ and CH₃OH were the main products in the gaseous and liquid phases. The CdS@CeO₂ combination resulted in more CH₄ and CH₃OH than CdS due to its lower photo-generated electron-hole pair recombination rate and larger BET-specific surface area. The core/shell configuration increases photocatalytic activity by isolating photo-generated charge carriers and limiting recombination. Photogenerated electrons from CdS to CeO₂'s CB may convert CO₂ to negative and metastable superoxide (\bullet CO₂⁻) radicals. This may produce CH₄ or CH₃OH. Since its potential is positive, photogenerated holes in the VB of CdS in the solution, such as H₂O and even a small amount of photo reduction products, may oxidize the reductant. Mengli Li et al. [88] established a novel mesostructured CeO₂/g-C₃N₄ nanocomposites with varied component ratios of 1–5 % mCeO₂/g-C₃N₄ by a simple rigid template technique, results remarkably improved CO₂ photoreduced product i.e., 0.590 CO and 0.694 μmol CH₄, for 3 % mCeO₂/g-C₃N₄, after one-hour irradiation on 50 mg nanocomposite photo-catalyst at room temperature. The highest light absorption and lowest electron-hole recombination efficiency were for 3 % mCeO₂/g-C₃N₄, and deactivation increased with Ce loading, likely because excessive Ce species have become charge carrier recombination centres and cover the catalytically active sites on catalysts surface byproducts and intermediates. A synergistic catalytic process for CO₂ photoreduction on m-CeO₂/g-C₃N₄ is expected: Photo-excited electrons from g-C₃N₄ to m-CeO₂ and their capture by Ce₄₊ prevent photogenerated electron-hole recombination. Meanwhile, m-CeO₂'s trapped electrons reduce Ce₄₊ to Ce³⁺ (CeO₂ activation), improving CO₂ reduction. It was successfully produced ordered mesoporous CeO₂ (m-CeO₂) by H. Wang et al. [89] by nanocasting method, using SBA-15 hard template. Additionally, calcination was used to successfully create the g-C₃N₄/Ag/m-CeO₂ composite. The XRD, SEM, and TEM results show that m-CeO₂ and Ag/m-CeO₂ display ordered mesoporous characteristics and the photocatalyst includes oxygen vacancies. Furthermore, the organized mesostructure facilitates the adsorption/desorption process and the mobility of CO₂. Ag, as a connection between m-CeO₂ and g-C₃N₄, shuttled electrons between the two semiconductors, enabling the transfer and separation of photogenerated transporters and extending their life, hence enhancing the photocatalytic activity of the obtained photocatalyst. Adding g-C₃N₄ nanosheets to Ag/m-CeO₂ inhibits the photo-corrosion of Ag nanoparticles. Most notably, Ag and CO have a lower binding capacity than other materials, allowing CO to desorb from Ag's surface. The photocatalytic activity of the g-C₃N₄/7Ag/m-CeO₂ (Ag 7 wt %) composite showed better effectiveness for CO₂ photoconversion to CO (13.94 μmol g⁻¹) and CH₄ (7.39 μmol g⁻¹) under UV-irradiation in 10 h.

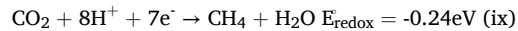
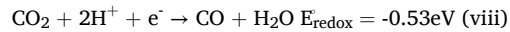
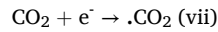
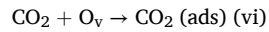
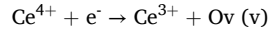
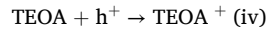
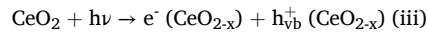
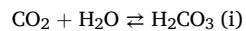
Yanan Wei et al.⁹⁰ effectively developed a composite photocatalyst co-modified with Au NPs and CN QDs and CeO₂/Fe₃O₄ Microflowers (MF) denoted as 1-CACeF, 2-CACeF, 3-CACeF, and 4–3-CACeF using hydrothermal calcination, deposit growth, and self-assembly methods. To begin, the different Ce⁴⁺/Ce³⁺ conversion mechanisms and the increased concentration of surface oxygen deficiencies of CeO₂ MFs facilitate the separation process of photogenerated carriers. The heterojunction at the CeO₂ MF/CN QD contacts promotes photogenerated electron transport. The composite's visible light adsorption capacity has also increased, presumably due to the many CN QD surface defects. Au NPs with a high local surface plasmon resonance (LSPR) effect improve the photocatalyst's photo-electron conversion efficiency. Furthermore, it promotes the production/separation of photogenerated carriers in CN QDs and CeO₂ MFs in the photocatalyst and the supply of hot electrons required for photocatalytic activity. The change in the structure of CN QDs enhances the composite photocatalyst's ability to absorb photons. Fe₃O₄ QDs enable photocatalyst recovery and reuse without impairing photocatalytic activity, and they also raise the catalyst's absorption edge

to roughly 720 nm. Electrons from CeO₂ MFs, CN QDs, or Au NPs with sufficient energy (-0.57 V) may then reduce the CO₂ molecules into CO (-0.53 V vs. NHE) and CH₄ (-0.24 V vs. NHE). Among all generated samples, 3-CACeF exhibited the highest photoreduction efficiency and stability.

Yangang Wang et al. designed ordered mesoporous CeO₂-TiO₂ composites on SBA-15 template, titanium tetrachloride, and cerium nitrate as sources with different compositions (Mes-CeTi-0.5, Mes-CeTi-1.0, and Mes-CeTi-2.0) for comparison with Mes-TiO₂ and Mes-CeO₂ [91]. They performed photocatalytic CO₂ reduction experiments under simulated solar light and structural investigation. Composites have red-shifted optical band gaps compared to Mes-TiO₂ and Mes-CeO₂, suggesting improved visible light absorption. XPS study showed increased surface oxygen species and a mix of Ce³⁺/Ce⁴⁺ states, suggesting photocatalytic reduction capacity and quantum efficiency.

A solvothermal approach was used for fabricating CeO₂/Bi₂MoO₆ heterostructure microspheres with stable CO₂ photoreduction activity by W. Dai et al. [92]. The as-prepared samples shape, phase, porosity, optical, chemical, and electrical properties are reported. CO₂ photoreduction mechanism study was also conducted. Thermodynamic viability of CO₂ photoreduction is shown by the reactive species, CO₃²⁻ and HCO₃⁻. The inclusion of CeO₂ on Bi₂MoO₆ increases CO₂ adsorption capacity, which may be converted into b-CO₃²⁻ and b-HCO₃⁻ species for photoreduction activity. The greatest yield of CH₃OH and C₂H₅OH with 5 C-BM was 58.4 μmol g⁻¹, 1.9 and 4.1 times higher than pure Bi₂MoO₆ and CeO₂, respectively. Additionally, CeO₂/Bi₂MoO₆ nanocomposites were highly recyclable and chemically stable.

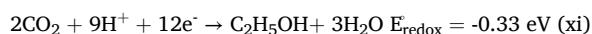
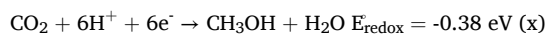
Several innovative porous indium (III) oxide (In₂O₃) and nanocubic cerium oxide (CeO₂) loading HCl-treated attapulgite (HATP) ternary photocatalysts with different In₂O₃ content (%) were synthesized in one step [93]. The names were 10In/Ce/HATP-x, 15In/Ce/HATP-x, and 20In/Ce/HATP-x. A heterostructure between porous In₂O₃ and CeO₂ nanocube increases photogenerated charge separation and transfer resulting in enhanced catalytic activity. Tri-ethanolamine (TEOA) also donates electrons and prevents electron-hole recombination on CeO₂ nanocubes, increasing the quantity of electrons for the process. After six hours, a 10In/Ce/HATP-20 heterostructure optimized for UV light irradiation generates 6.11 and 6.78 times more CO and CH₄ for CO₂ reduction than pure CeO₂ nanocube. Based on the description, these equations reflect the main conversion process:



With starting Zn/C molar ratios of 0.5, 1.0, and 2.0, ZnO/CeO₂ nanocomposites were developed via a single-step flame spray pyrolysis (FSP) process [94]. The findings of the TEM and BET analyses show that adding CeO₂ decreases particle size and increases the surface area of the nanocomposites. In addition, ZnO's light response is effectively extended to the visible range by the incorporated CeO₂ species. Meanwhile, the ZnO in the composites increases the concentration of surface hydroxyl groups on the catalysts and enhances the interaction between CO₂ and the composites. The formation of the ZnO/CeO₂ heterojunction and the co-existence of Ce⁴⁺/Ce³⁺ significantly enhance the separation

of photogenerated electron-hole pairs inside the composites. For CH₄ and CO, the calculated quantum yields for ZnCe-1 were 0.51 % and 0.27 %, respectively. The fact that these values are significantly higher than those for ZnO and CeO₂ indicates that the photon utilization efficiency of ZnO/CeO₂ composites is higher.

Another ternary photocatalyst was reported by Panpailin Seeharaj et al.; it was achieved by combining CeO₂, rGO, and titanium dioxide (TiO₂) nanoparticles with surface modification [95]. The TiO₂ surfaces were initially modified by sonoassisted exfoliation (20 kHz, 150 W cm⁻²) using high-intensity ultrasonic waves in 10 M NaOH for an hour. A combination of 0.75 wt% rGO and 1 wt% CeO₂ was added to the surface-modified TiO₂ to improve CO₂ absorptivity, electron mobility, and photogenerated charge separation. The modified TiO₂/rGO/CeO₂ photocatalysts produced methanol (641 μmol g⁻¹) at over 7 times than the methanol production rate of pure TiO₂, whereas the ethanol production rate is 271 μmol g⁻¹. The process of photoconverting CO₂ to methanol and ethanol is shown by equations.



Modified TiO₂/rGO/CeO₂ coupled produced complex heterojunction photocatalysts with a decreased band gap, high surface area (83 ± 5 m² g⁻¹), and strong phase connections; these features greatly increased CO₂ photoconversion rates.

2.3.3.3. p-n heterojunctions. The type II procedure aligned with the p-n type heterojunction's probable photoreduction mechanism. On the p-n type heterojunction interface, a localized internal electric field was produced with an orientation from n-type to p-type semiconductor, as depicted by Fig. 4B. Until the equilibrium state was reached, holes traveled in the opposite direction from the photogenerated electrons as they migrated from the CB of the p-type semiconductor to the n-type semiconductors due to the electrostatic interaction. The opposing motion of electrons and holes limited the recombination probability. When exposed to visible light, the separated electrons and holes act as reducing and oxidizing agents. When water molecules are reduced to CO₂, the holes produce protons and electrons, which combine with the available protons to form methanol. When an external voltage is

supplied, the heterojunction's internal charge opposes it, increasing the conductivity in the interfacial region. Because of this, forming p-n heterojunctions is highly advantageous for promoting interfacial charge transfer and increasing charge carrier mobilities, [98,100] In this study, a Fe-Ni@CeO₂ nanocomposite photocatalyst (FNC) was synthesized. Fe₃O₄ nanospheres (Fe NSs) were decorated using a template on CeO₂ nanorods (NRs). An aqueous ammonia solution of nickel chloride was used to deposit NiO hexagonal nanoparticles (Ni HNPs) post sol-gel hydrothermally. The catalyst used triethylamine (TEA) as a sacrificial donor and water as a proton source at room temperature (RT) under visible light to selectively reduce CO₂ to methanol. FNC heterojunctions absorb more visible light and have a lower band gap of 2.13 eV. The progressive decoration of CeO₂ NRs with Fe₃O₄ NSs and NiO HNPs lowers the band gap. Electrons flow from CeO₂ to NiO in the FNC composite's n-p heterojunction. Developing an electric field can produce up to 7039 μmol g⁻¹ of methanol in 24 h of radiation exposure. When exposed to visible light, semiconductors separated charge, stabilizing photogenerated holes and electrons at CB and VB. Photogenerated electrons from NiO's CB were transported to CeO₂. Water molecules delivered protons and electrons into CeO₂'s VB holes. PL spectra of the FNC heterojunction supported the hypothesis that the remaining holes went to VB of NiO due to the electric field that inhibited CeO₂ electron-hole pairs from recombining. When exposed to visible light, CeO₂'s CB electrons went to Fe₃O₄ NSs, where they reduced CO₂ and produced CH₃OH with protons. The excellent separation of electron-hole pairs by the FNC heterojunction device improved CO₂ reduction-derived methanol production. Zhengbin Pan et al. developed a photoelectrocatalytic catalyst Flowerlike p-n heterojunction of n-type CeO₂ and p-type CuO for selective CO₂ to CH₃OH reduction [97]. The CeO₂ NPs/CuO NPs/Cu catalyst produced 3.44 μmol cm⁻² h⁻¹ of methanol under visible light, about five times more than the 0.67 μmol cm⁻² h⁻¹ produced by a CuO NPs/Cu catalyst at -1.0 V (versus SCE). The Mott-Schottky equation determined the acceptor concentrations (NA) for the flower-like CeO₂ NPs/CuO NPs catalyst and the CuO NPs catalyst. Results indicate NA values of 3.47 × 10⁻⁵ and 2.93 × 10⁴ m⁻³, based on fermi levels for each electrode. The Ce 3d XPS spectrum shows several Ce⁴⁺ and Ce³⁺ peaks. Sol-gel synthesis yielded nanocomposite photocatalysts with 5, 10, 15, and 20 wt% p-type bismuth oxide (Bi₂O₃) and n-type CeO₂ [98]. Photoluminescence, photocurrent, and optical

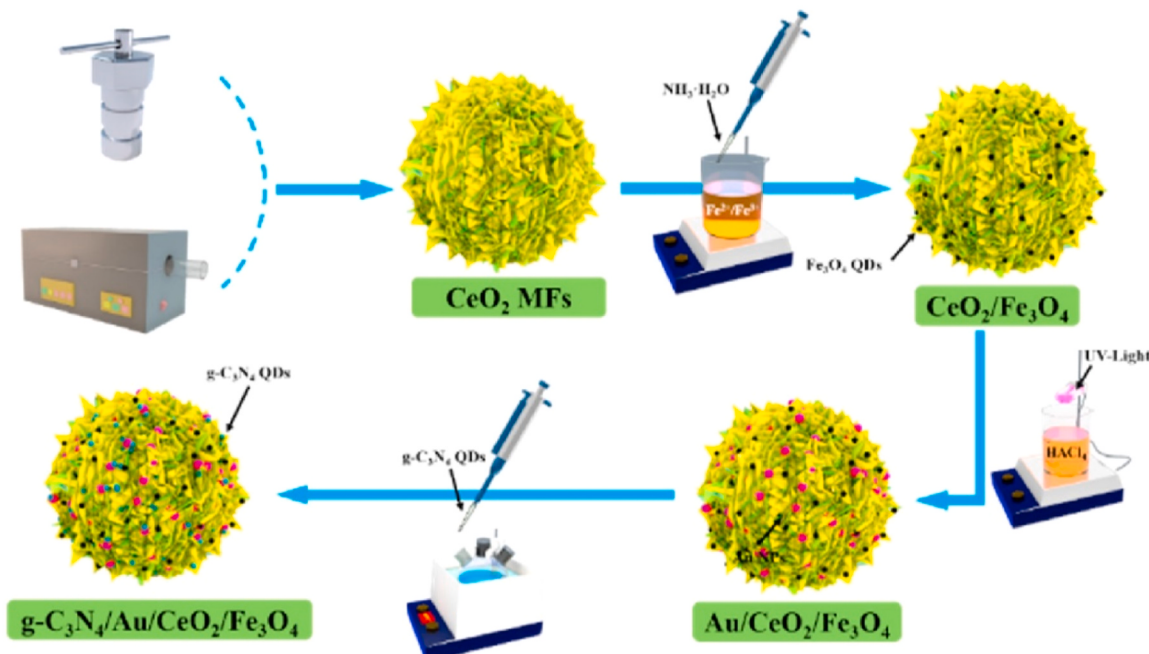


Fig. 5. Fabrication steps of g-C₃N₄/Au/CeO₂/Fe₃O₄ (CACeF). Reproduced (adapted) from [90] Copyright 2021, Elsevier.

response measurements showed that larger charge separation enhanced visible light absorbance. For 15 % $\text{Bi}_2\text{O}_3/\text{CeO}_2$, the total bandgap dropped to 2.75 eV from 2.93 eV for pure CeO_2 . The adjusted g L^{-1} dose of 15 % $\text{Bi}_2\text{O}_3/\text{CeO}_2$ with the maximum photocurrent value ($51.54 \mu\text{A cm}^{-2}$) selectively derived $1300 \mu\text{mol g}^{-1} \text{CH}_3\text{OH}$ after 9 h of visible light exposure. Nanocomposite photocatalysts' photoactivity depends on adjusting the dosage because photoactive spots increase in balance with light photons and adsorbed target molecules. Also, this photocatalyst is five times recyclable.

2.3.3.4. Z-schemes. The Z-scheme mechanism of CeO_2 -based hybrids as shown in Fig. 4C, involves the transportation of photogenerated e^- from the CB of CeO_2 to the VB of SC1 for h^+ consumption and the energy emitted as heat and futile light. The Z-scheme charge transfer mechanism enhances photoinduced electron and hole separation in heterostructures, even with higher redox potentials for left e^- and h_+ . Muhammad et al. [99] developed hierarchical flower-like ternary layered double hydroxides (LDHs) of $\text{NiFeCr-LDH-(PCN/CeO}_2$) by incorporating 5 %, 10 %, 15 %, and 20 % PCN/ CeO_2 . The hierarchical heterostructure that mimics a flower exposes more surface-active areas, enhancing light harvesting. The composite $\text{NiFeCr-LDH-(PCN/CeO}_2$ -15 %) showed impressive photocatalytic activity, forming CO and CH_4 at 52.1 and $17 \mu\text{mol g}^{-1}\text{h}^{-1}$, respectively, with high selectivity. Radiation stimulates PCN/ CeO_2 and NiFeCr-LDH to produce electrons and holes, explaining this composite's photocatalytic Z-scheme process. After transferring photogenerated electrons to the VB of PCN/ CeO_2 , the CB of NiFeCr-LDH combines with the photogenerated holes. This may cause holes and electrons to accumulate on PCN/ CeO_2 's CB and NiFeCr-LDH's VB. Thus, the photocatalyst's oxidation and reduction capability increases, improving photoinduced exciton separation. Coupled with a hierarchical flower-like structure, it allows the synthesis of LDH-based heterostructures for CO_2 . Thus, combined with a unique hierarchical flower-like structure, it allows the synthesis of heterostructures based on LDHs that reduce CO_2 by improving charge carrier separation and light-harvesting capacity, increasing photocatalyst adsorption and activation. A novel $\text{Cu}_2\text{O}/\text{WO}_3/\text{CeO}_2$ (CuWCE) ternary metal oxide cascade Z-Scheme nano-heterostructure has been demonstrated by Prajapati et al. [100] by hydrothermal method for CO_2 photoreduction to CH_3OH under visible light. $\text{Cu}_2\text{O}/\text{WO}_3/\text{CeO}_2$ (CuWCE) ternary composite exhibits a four times greater CH_3OH production rate than WO_3/CeO_2 binary oxide components and eight times

greater than pure CeO_2 without any co-catalyst. CeO_2 , WO_3 , and Cu_2O exhibited absorption edges of 450, 488, and 645 nm, respectively, with bandgaps of 2.75, 2.54, and 1.92 eV. CuWCE ternary metal oxide had a bandgap of 2.14 eV, suggesting its higher photoactivity. The BET surface area of CuWCE nanocomposite was $53.81 \text{ cm}^2 \text{ g}^{-1}$, compared to 62.13 for CeO_2 . The effect of sacrificial agent and solvent on photoactivity was investigated as well. DMF generates more methanol than CH_3CN as a solvent because it absorbs more CO_2 . The sacrificial agent TEOA has three -OH groups at the 2nd ethyl moieties. The photoreduction of CO_2 lowered methanol production because the lone pairs at the N-atom of TEOA did not serve as donors owing to the -I action of -OH groups on ethyl. Due to the +I effect and three ethyl groups at the N-atom, TEA produces more methanol than TEOA in the same circumstances. You-Xiang Feng et al. synthesized 2D lead-free halide perovskite ($\text{Cs}_3\text{Bi}_2\text{I}_9$) nanosheets using $\text{BiOI/Bi}_2\text{O}_{2.7}$ nanosheets as the template and Bi ion source [101]. A Z-scheme heterojunction of $\text{Cs}_3\text{Bi}_2\text{I}_9$ and CeO_2 nanosheet ($\text{Cs}_3\text{Bi}_2\text{I}_9 / \text{CeO}_2$ -3:1) was developed as a photocatalyst for CO_2 photo-reduction in H_2O using electrostatic self-assembly. The composite's photogenerated carrier separation efficiency was enhanced due to the $\text{Cs}_3\text{Bi}_2\text{I}_9$ and CeO_2 nanosheets' matching energy levels and tight interfacial contact. Hence, the eco-friendly halide perovskite heterojunction ($\text{Cs}_3\text{Bi}_2\text{I}_9 / \text{CeO}_2$ -3:1) outperforms other bismuth-based perovskites in photocatalytic CO_2 reduction, with an electron consumption yield of $877.04 \mu\text{mol g}^{-1}$, 7 and 15 times higher than pristine $\text{Cs}_3\text{Bi}_2\text{I}_9$ and CeO_2 nanosheets.

Hydrothermal synthesis of $\text{SnS}_2/\text{CeO}_2$ heterojunction composite photocatalysts (molar ratios $\text{CeO}_2:\text{SnS}_2 = 10\%, 20\%, 30\%$, and 40%) combined the oxygen vacancies and electric field of SnS_2 and CeO_2 [102]. Using various characterization techniques, the photocatalyst's structure was examined, and oxygen vacancies and heterojunction structure were found to improve photocatalytic performance and carrier transport efficiency. Unpaired electrons may result from oxygen vacancies. Dopant centers, dangling bonds, and defects have unpaired electrons. Thus, EPR spectra may indirectly prove oxygen vacancies exist. CeO_2 and ($\text{CeO}_2:\text{SnS}_2 = 40\%$) composites showed strong EPR spectra. However, pure SnS_2 had nearly zero signal. Two-dimensional SnS_2 nanosheets are loaded with zero-dimensional CeO_2 nanoparticles to form a 2D/0D structure that improves photo-response range and electron transfer rates. The composite material conserved SnS_2 's hydrophobicity while avoiding CeO_2 's hydrophilicity. Oxygen vacancies are another vital element in photocatalytic CO_2 reduction effectiveness,

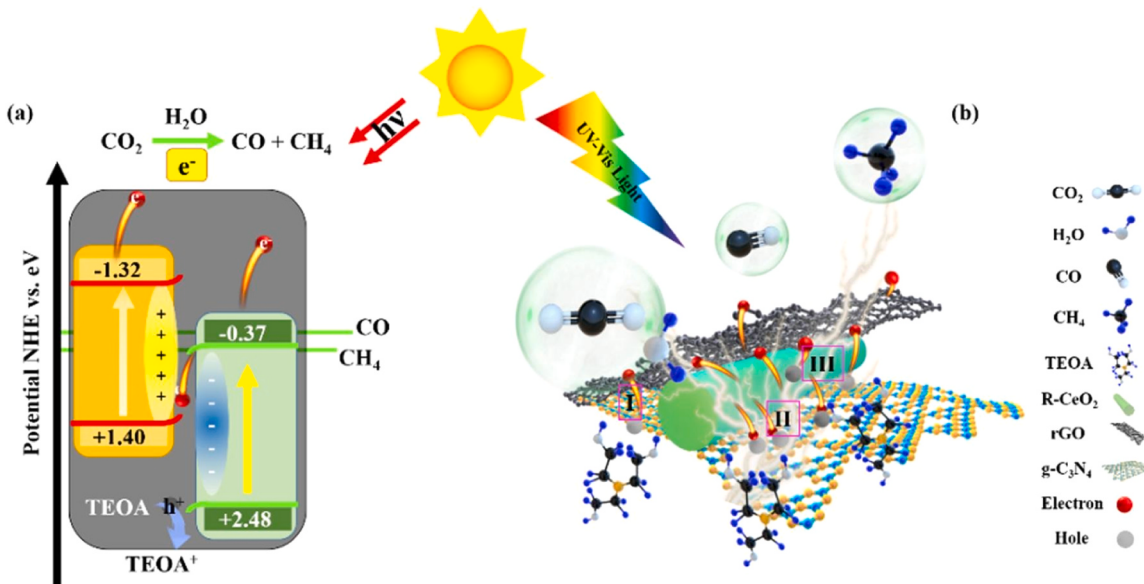


Fig. 6. a) The band gap structure and b) a schematic of 3RCCN multi-interface contact composite photocatalyst for CO_2 photoreduction under UV-vis light. Reproduced (adapted) from [105] Copyright 2021, Elsevier.

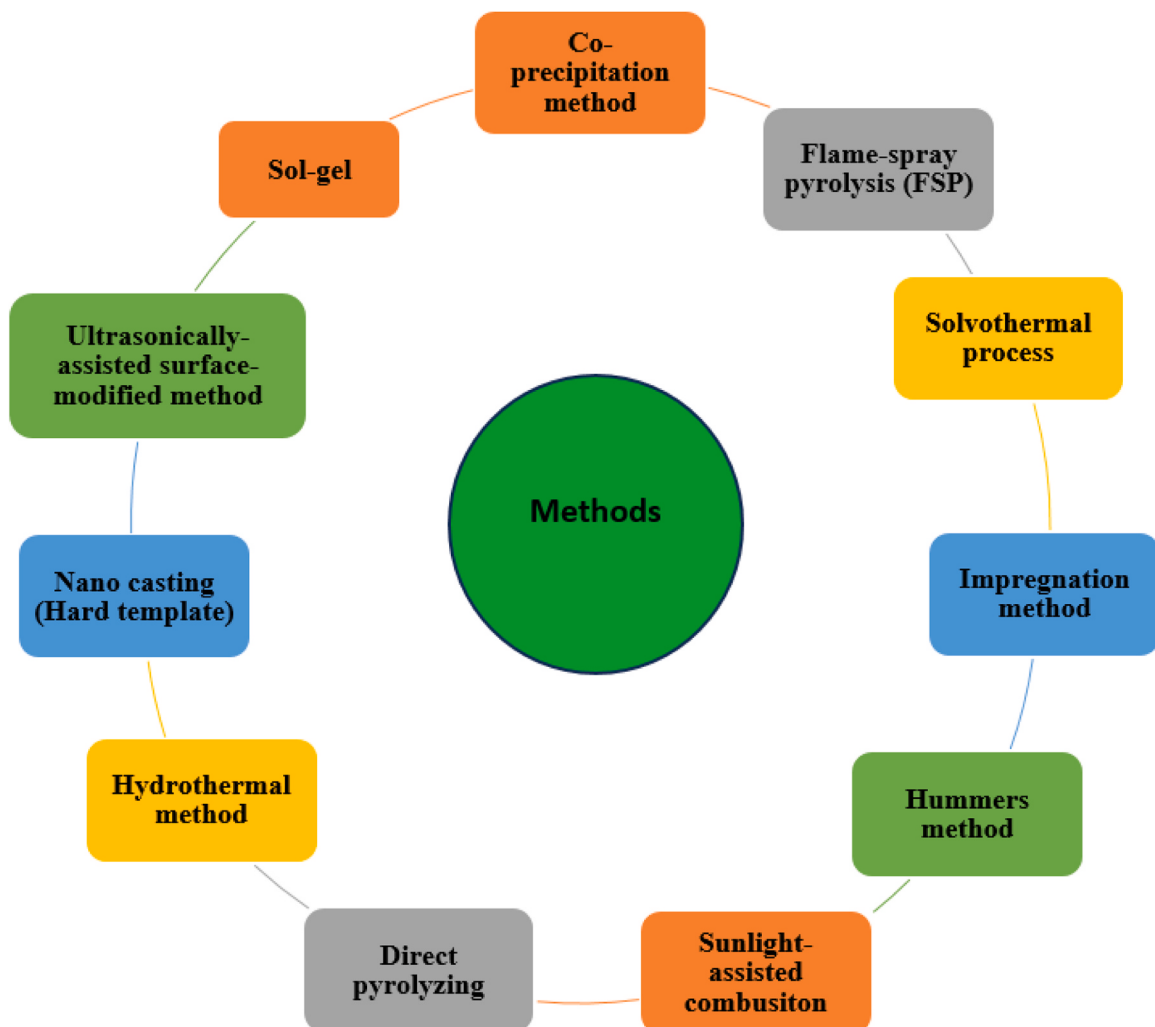


Fig. 7. Different methods for the synthesis of CeO₂-based photocatalysts for CO₂ reduction.

which diminishes CO₂ molecule adsorption potential. Hydrophobic features of the SnS₂/CeO₂ composite photocatalyst reduce water molecule occupancy of active sites, reducing CO₂ adsorption competition. This hydrophobic surface allows CO₂ molecules to enter the liquid phase system and adsorb on the photocatalyst. Thus, the binary Z-type heterojunction photocatalyst generated 24.6 and 4.4 times more CO and CH₄ by water molecules than single SnS₂, reducing CO₂ adsorption competition on the catalyst surface. This hydrophobic surface allows CO₂ molecules to enter the liquid phase system and adsorb on the photocatalyst. Compared to single SnS₂, the binary Z-type heterojunction photocatalyst produced 24.6 and 4.4 times more CO and CH₄. This important research will advance SnS₂-based photocatalytic materials and provide an innovative way to light energy-driven CO₂ reduction. To reduce CO₂ photocatalytically, phosphate-modified octahedral CeO₂ {111} surface coupling with g-C₃N₄ (P-CeO₂/g-C₃N₄) was developed. It was more active than P-CeO₂, g-C₃N₄, and CeO₂/g-C₃N₄ [103]. First, FT-IR, ¹H, and ³¹P solid-state MAS NMR investigated P species coordination environments. The bridge function of PO₄³⁻ was revealed by XPS and DFT simulations of interfacial electronic interactions. Characterization demonstrated the coordination environment of P species and a hydrogen connection between phosphate and amino. CO₂-TPD data shows a large peak in the 50–450°C temperature range due to CO₂ adsorption on the catalyst surface and reaction intermediates (carbonate species). The wide peak has been divided into bicarbonates (b-CO₃²⁻, 370–550 °C), monodentate carbonates (m-CO₃²⁻, 550–7780 °C), molecule-adsorbed CO₂ (50–180 °C), and HCO₃⁻ or carboxylate (180–370

°C). In-situ CO₂adsorption DRIFTS under light irradiation were eventually found to demonstrate the reaction mechanism for CO₂ photocatalytic reduction and the favorable impact of PO₄³⁻ in reaction sites. The Z-scheme and fast photogenerated charge transfer were triggered by interfacial electrons from g-C₃N₄ to CeO₂ via the PO₄³⁻ bridge. The PO₄³⁻modified surface also increased the amount of oxygen-containing functional groups that were Lewis basic sites for CO₂ reactant adsorption and activation. Due to its plentiful active sites and charge-transfer channel, P-CeO₂/g-C₃N₄ may reduce CO₂ as a photocatalyst. This leads to the greatest CO generation rate of 4.184 μmol g⁻¹, surpassing 3.5, 5, 1.6, and 1.8 times g-C₃N₄, CeO₂, P-CN, and P-CeO₂. Engineering and designing plasmonic metal nanocomposite photocatalysts may reduce CO₂ effectively. The authors reported a plasmonic flower-like 3D Ag–CeO₂–ZnO (3DF) nanocomposite. Its charge separation/transfer and CO₂ adsorption capability are superior to pure ZnO and CeO₂ for photocatalytic CO₂ reduction to CO and CH₄ in the UV-vis region [104]. The obtained samples were labeled xAgCZ, where x = 1, 2, 3, and 4 % represents the Ag mass ratio. The heterostructures' band gaps for 1AgCZ, 2AgCZ, AgCZ, and AgCZ with different Ag concentrations were 3.17, 3.12, 2.91, and 3.02 eV, respectively. As Ag content increases, CO and CH₄ production rates increase. After five hours of light irradiation, 3AgCZ at a concentration of three mg of Ag per litre increases CO generation and CH₄ production by 377.52 and 20.12 μmol g⁻¹, respectively. The optimized sample 3AgCZ exhibits 4.47 % apparent quantum efficiency and 95 % CO₂ to CO selectivity at 420 nm. The synergistic effects of expanded visible absorption, the Surface Plasmon Resonance (SPR)

effect, and the Z-scheme system, which enhances photogenerated transporter separation, use important electrons and holes, and optimizes the redox potential, improve photocatalytic performance. This study suggests new semiconductor-based plasmonic multicomponent photocatalytic CO₂ reduction device architectures.

2.3.3.5. S-Scheme. Multi-interface contact step-scheme (S-scheme) photocatalyst preparation may also achieve high-electron transfer effectiveness UV-vis light-assisted CO₂ reduction (Fig. 6). Xin Li *et al.* [105] developed a ²D-¹D-2D sandwich photocatalyst using g-C₃N₄ nanosheets as the primary photocatalyst and loaded rGO and R-CeO₂ (with special Ce⁴⁺→Ce³⁺ conversion property) on the surface. Using rGO/R-CeO₂/g-C₃N₄ as a catalyst resulted in CO and CH₄ yields of 63.18 and 32.67 μmol g⁻¹ after 4 h. These were 4–6 times higher than pure CN. The composite showed excellent photocatalytic and material stability in cyclic testing. Since the specific work function ($\Delta\Phi$) of photocatalyst materials differs, density functional theory suggests that electrons from g-C₃N₄ with lower $\Delta\Phi$ must move to CeO₂ with higher $\Delta\Phi$ until their E_f level out. Thus, CeO₂ will have an electron-accumulation region and g-C₃N₄ a hole-aggregation area. Electron and hole buildup bends g-C₃N₄ and CeO₂ band boundaries upward and downward. The contact between the two charge zones also produces a built-in electric field from g-C₃N₄ to CeO₂. Electrons from the CB of CN can transfer to the surface of rGO via the Schottky-like barrier. R-CeO₂ CB electrons can rapidly recombine with holes on the VB of CN through the ¹D-²D contacted interface (III), following the same path as in (I). Another portion of the electrons can transfer to the surface of rGO via the 1D-2D Schottky-like barrier interface. The S-scheme electron transport model and rGO showed promise in photoelectrochemical testing. The R-CeO₂'s Ce⁴⁺ ion may also capture electrons and be reduced into Ce³⁺, which helps separate photogenerated carriers. The CO₂-adsorption studies show that R-CeO₂ and rGO significantly improve the photocatalyst's CO₂ absorption capability. This may be because both surfaces have functional groups and defects. The rGO/R-CeO₂/g-C₃N₄ hybrid photocatalyst may be used as a model for S-scheme multi-dimensional/multi-interface contact photocatalysts for CO₂ photoreduction. Table 4 shows CO₂ photocatalytic reduction results using CeO₂-based nanocomposite photocatalysts.

3. Synthesis methods of CeO₂-based photocatalysts

CeO₂-based photocatalysts can be synthesized using various methods, including co-precipitation, nano-casting, hydrothermal, and sol-gel methods. Co-precipitation offers a straightforward synthesis step but produces low purity, large particle size, and poor dispersion [45, 106–109, 21, 32]. Sol-gel has high purity and excellent catalytic properties but incurs higher costs due to expensive metal alkoxides [106]. The template method allows precise control of size, structure, and morphology of CeO₂-based nanomaterials but has drawbacks like low processing efficiency and strict process conditions that limit its application in photocatalysis [107]. Methods used for synthesizing different photocatalysts have been included in the tables (Tables 2, 3, and 4). In most cases, preparing a complex photocatalyst includes different methods for doping or modification.

The sol-gel method is a chemical technique used to produce hollow-shaped CeO₂ nanomaterials. This process involves the hydrolysis of precursors, such as metal alkoxides, followed by condensation to form a transparent sol system with stable properties. The resulting wet gel is dried or treated to produce the crystalline phase. This method facilitates homogeneous mixing of dopants at the molecular level, making it particularly useful for modifying CeO₂ with metal or non-metal dopants [106]. However, the calcination process required to form the crystalline material can result in grain growth, particle agglomeration, and a reduction in surface area. Mostafa *et al.* synthesized nanocomposite photocatalysts that are active under visible light containing CeO₂ and

bismuth oxide (Bi₂O₃, 5.0–20.0 wt%) using a sol-gel- process [98]. Additionally, Anna Corrias and her team developed CeO₂-SiO₂ aerogel nanocomposites by using cerium (III) nitrate as a precursor for CeO₂ and controlling the growth of CeO₂ nanoparticles within a silica aerogel matrix [110].

The hydrothermal method typically involves conducting reactions in aqueous solutions within autoclaves lined with Teflon under controlled temperature and pressure [106]. In contrast, the solvothermal approach uses a non-aqueous solution. Due to the high pressure in the sealed reactor, the solution's temperature can be raised above its boiling point, reaching the vapor saturation pressure. Under these conditions, optimizing hydrothermal parameters (such as temperature and time) can produce photocatalysts with small crystal sizes and high specific surface areas [106]. Many photocatalysts reported for solar-driven photoreduction are synthesized using the hydrothermal method. Examples include g-C₃N₄@CeO₂ [105], 3D Ag-CeO₂-ZnO heterostructures [104], SnS₂/CeO₂ heterojunction composites [102], g-C₃N₄ quantum dot/mesoporous-CeO₂ [83], NiFeCr-LDH-(PCN/CeO₂) heterostructures [99], composite CeO₂/Fe₃O₄ MFs co-modified with Au NPs and CN QDs [90], In₂O₃/CeO₂/HATP hybrid multi-junctions [93], phosphate-decorated octahedral CeO₂/g-C₃N₄ [103], 3D flower-like Ag-ZnO-CeO₂ (AgCZ) [104], Er-doped CeO₂/rGO/CuO [67], and Y, La, and Mo-doped CeO₂ [63]. Additionally, Ijaz *et al.* used the hydrothermal method to synthesize CeO₂ and CdS, followed by a two-step chemical process to prepare the CdS@CeO₂ composite [87]. The solvothermal method is also used to synthesize photocatalysts, such as CeO₂/Bi₂MoO₆ [92] and CdS/mesoporous CeO₂ catalysts [49] for CO₂ reduction to fuel.

On the other hand, co-precipitation is a simple, low-cost, and widely used method for CeO₂-based photocatalyst preparation. It combines precipitants, surfactants, metal resources, and heat treatment. Mild alkaline substances like urea and amine are used, releasing OH ions to facilitate mixed-metal oxide precipitation [107, 111]. However, controlling particle size and morphology is challenging. For example, Zr doped CeO₂ [64], and BiOCl/CeO₂ composite [6] use mild conditions and ethylene glycol as a solvent.

The template method is a simple and efficient method for preparing CeO₂ hollow structures by sacrificing the material route. It uses the stability contrast between the target material and its template, allowing the core to be removed while preserving the shell. This method can be classified into hard templates and soft templates, offering precise control over size, morphology, and structure [107]. Mengli Li *et al.*, demonstrated a simple hard template method for preparing mesostructured CeO₂/g-C₃N₄ nanocomposites, which exhibits significant light sensitivity, efficient separation and charge transfer across the interface between g-C₃N₄ and mesoporous CeO₂ [88]. SBA-15 was used as a hard template to effectively fabricate composite made of g-C₃N₄, Ag, and m-CeO₂ [89]. Golovanova *et al.* (2021) also used SBA 15 template to synthesize the Ni/CeO₂ catalyst [82]. A similar method was used in synthesizing Fe-Ni@ CeO₂Nano rods (FNC) [96], Cs₃Bi₂I₉/ CeO₂-nanosheets [101], Chromium doped mesoporous CeO₂⁶² and g-C₃N₄/Ag/CeO₂-mesoporous photocatalysts [89].

In addition to these widely used techniques, there are some alternative methods. For example, flame spray pyrolysis (FSP) is a simple and convenient method for synthesizing binary metal oxide nanocomposites in a single step, unlike wet chemistry routes. Xiong *et al.* (2017) used one-step FSP to synthesize ZnO/CeO₂ nanocomposites of different molar ratios, demonstrating the versatility of flame synthesis in catalyst synthesis [94]. Seeharaj *et al.* modified TiO₂ surfaces via sono-assisted exfoliation with high-intensity ultrasonic waves to prepare TiO₂/r-GO/CeO₂ composite photocatalysts [95]. By using a straightforward high-temperature calcination process, a spindle-structured CeO₂ photocatalyst modified with rod-like attapulgite (CeO₂/ATP) was effectively synthesized by Zheng *et al.* After adding ATP to the CeO₂ precursor solution, the mixture was heated to produce the CeO₂/ATP photocatalyst [81]. Cui *et al.* (2020) synthesized g-C₃N₄ using dicyandiamide thermal

polymerization at 600°C and constructed a g-C₃N₄/CeO₂ heterojunction, whereas Zhou and Liu (2017) applied Hummers' method to incorporate nitrogen atoms on a graphene frame using an imidazole cycle and prepared Cu(II)/ING/CeO₂ catalyst [84]. CeO₂ nanoparticles were dispersed on ING sheets, creating an ING/CeO₂ hybrid material. Moreover, Sulphur-doped carbon coated In₂O₃-CeO₂ hollow hexagonal prism (S-C/ In₂O₃-CeO₂ HHP) was synthesized by directly pyrolyzing Ce-doped In-MIL-68 hexagonal prism metal-organic frameworks under N₂ atmosphere in the presence of sulfur powder [71]. Pan *et al.* developed a CeO₂/CuO catalyst for selective CO₂ reduction to methanol using an electrochemical method [97].

4. Factors affecting the reduction of CO₂

4.1. Band gap of photocatalyst

UV radiation accounts for just 5 % of the solar spectrum, making large bandgap photocatalysts effective. As a consequence, there is a low yield of solar products [112]. Mesoporous CeO₂ (NM Ce) doped with nitrogen exhibited reduced band gap energy, improved CO adsorption ability, and increased surface Ce³⁺ concentration with increased oxygen vacancies. The photocatalytic activity was better due to its broader light spectrum response and lower charge recombination [113].

4.2. Doping

The structure of a semiconductor photocatalyst, especially its bandgap, may vary due to element doping. Doping with metals and nonmetals often adds amounts over or below the VB threshold, influencing the photoelectric characteristics of semiconductors. Doping-based modification has been shown to be an effective technique for increasing the efficiency of photocatalytic processes [113].

4.3. Morphology of the photocatalyst

The charge transport and recombination rates of the process are mostly determined by the features of the photocatalyst, such as its shape, crystal structure, and particle size. The enormous number of atoms at the surface and their unique optical, crystallographic, and electronic characteristics make the nanometric dimension essential for a semiconducting material to act as an effective photocatalyst. Because of the remarkably enhanced qualities of nanomaterials, the photocatalytic effectiveness has grown with size reduction from the bulk form to nanoparticles.

When compared to bulk materials, nanomaterials with a larger surface area and smaller size (less than 100 nm) often have quicker charge transport and recombination rates, which will ultimately improve photocatalytic efficiency. The shape of the materials used as photocatalysts greatly influences charge carrier dynamics. For example, one-dimensional (1-D) materials with intriguing morphologies like nanorods, nanowires, and nanocubes have a lot of surface defects, more active oxygen species, and excellent reducibility [32]. The semiconductor crystal phase plays a role in influencing a material's product selectivity. Modifications or alterations in the crystal phase might result in minute variations in band location. This is caused by atomic coordination and geometries variation which alter electronic states and the inherent kinetics of e-/h+ recombination [114].

4.4. Effect of light intensity

The electronic transition, which is connected to light intensity, influences the amount of electrons in excited states, and as light intensity rises, so does the rate of CO₂ reduction [32]. No product was produced in the absence of light during CO₂ reduction using the C₃N₄@CeO₂ nanocomposite. On the other hand, the rate of hydrocarbon (i.e., CH₃OH, CO, CH₄) formation rises with time with the addition of light [32].

High-power lights emit multiple photons, which produce electron-hole pairs on photocatalyst surfaces. The production of hydrocarbon from CO₂ reduction rises with light intensity, but decreases with wavelength as temperature increases [115].

4.5. Temperature

The kinetic energy of molecules, discussion of reactants, and product desorption rate of reaction increases with temperature [112]. Higher temperatures facilitate effective charge transfer, enhancing CO₂ reduction, with optimal reduction occurring between 80 and 100 °C [116].

4.6. Pressure

Adsorption of CO₂ molecules is influenced by van der Waals forces, which increase with partial pressure, affecting the likelihood of adsorption over photocatalysts in gas and liquid phase systems [112]. When operating under high CO₂ pressure, kinetic control of the reaction may be obtained, but at lower pressure, dissolution equilibria significantly limit the reaction rate [117].

4.7. Initial CO₂ Concentration

The product yield can be increased by providing high concentration of CO₂ in its photoreduction [118]. The initial concentration of CO₂ has an influence on the product selectivity i.e., a high concentration of CO₂ prefers CO, CH₄, CH₃OH etc. while a low CO₂ concentration produces CH₄ and a small amount of CO [119].

4.8. Effect of pH

At low pH, proton reduction to hydrogen dominates, while increased pH improves CO₂ reduction reaction rates, especially hydrocarbon generation. High pH decreases local CO₂ concentration due to higher reaction rates, while lower proton availability slows hydrocarbon generation due to higher local pH [120]. The pH value influences CO₂ solubility and concentration of CO₃²⁻, HCO₃⁻ and molecular CO₂, resulting in different adsorption modes. Higher pH causes CO₂ to hydrate, forming carbonic acid partially and may dissociate into carbonate and bi-carbonate [120].

4.9. Effect of Surface Functional Groups

Functional groups significantly contribute to CO₂ reduction by providing basic sites for CO₂ attraction or causing surface hydrophobicity to repel H₂O, generating intermediates like carbonate that easily reduce to various products [112]. Monodentate carbonate (m-CO₃²⁻), bidentate carbonate (b-CO₃²⁻), and bidentate bicarbonate (b-HCO₃⁻) are the primary surface species for the co-adsorption of CO₂ and H₂O on TiO₂ and CeO₂/TiO₂. The photocatalyst surface becomes stronger due to CeO₂ containing Ce³⁺ increasing the production of b-CO₃²⁻ and b-HCO₃⁻ surface species, which readily transformed to surface CO₃²⁻ in the presence of water under simulated sunlight irradiation [121].

4.10. Reducing agent

When water is used as a reducing agent in CO₂ reduction products like CH₃OH, C₂H₅OH predominates. Seeharaj *et al.* showed TiO₂/rGO/CeO₂ heterojunction photocatalyst produced CH₃OH and C₂H₅OH by reducing CO₂ with water ⁹⁵. Use of NaOH, NaHCO₃, etc. favored the formation of CO, CH₄, etc. For example, In₂O₃/CeO₂/HATP nanocomposite produced CO (32.03 μmol/g) and CH₄ (16.94 μmol/g) by using NaOH as a reducing agent.

4.11. Effect of design of the reactor

Photoreactor	Properties	Effect	Reference
Fixed bed reactors	Enhance light exposureIncreased interaction between catalyst	Improve CO ₂ reduction	
Optical fiber reactors	limited volume utilization efficiency (20–30 %)small surface area limited strength of catalyst adherence on the fibre	It has drawbacks (an alternative monolith type reactor can be used in combined)	[122]
Fluidized bed reactors	Photocatalysts are dispersed in aqueous mediumH ₂ O, NaOH, and Methanol are the solvents	Improved CO ₂ reduction depending on the reducing agent to which CO ₂ reacts.	[123]
Membrane reactors	Individual and controlled reactionH ₂ O is reducing agentFinal products are CH ₃ OH and C ₂ H ₅ OH	Improve CO ₂ reduction with good product selectivity	[123]

5. Challenges and future perspectives

An exceedingly promising method involves the photocatalytic conversion of CO₂ into valuable fuels by harnessing abundant solar energy. CeO₂ and its blends have shown potential as photocatalytic materials for this conversion process. This study assesses the research and advancements focused on enhancing the photoactivity of conventional CeO₂ under visible light and addressing its limitations. Several studies have examined specific techniques for modifying materials, including the integration of additional semiconductor nanostructures, the formation of oxygen vacancies, and the introduction of doping agents with or without metals. As a result, significant progress has been made in the change of CeO₂ to improve the efficiency of converting CO₂. Although CeO₂ and CeO₂-based photocatalysts have received significant attention and have shown various favourable effects in recent years, there are still problems that need to be addressed.

CeO₂ has a large bandgap, which restricts its photoreactivity despite its several advantages, such as stability, reusability, and environmental friendliness. This restricts its use to UV light, which is regarded to be dangerous and energy-intensive. Thus, there is a great deal of interest in developing and producing enhanced CeO₂-based photocatalysts to increase visible light absorption. Several newly discovered CeO₂-based photocatalysts have been employed for CO₂ photocatalysis. This suggests that the development of composite photocatalysts with complex compositions and designs may significantly accelerate the conversion of solar energy into chemical energy.

Accurately controlling the size, shape, and interface composition of CeO₂-based composites remains difficult. As a result, it is critical to create novel synthetic processes and get a better knowledge of the mechanisms involved in material production.

There are still significant gaps in our understanding of how to produce high-value hydrocarbon products. In addition, it is crucial to thoroughly assess the conversion efficiency of photocatalysts and the selectivity of products from CO₂ photoreduction to enhance the yield of valuable hydrocarbons and reduce the cost of product separation. By comprehending the reduction mechanism of CO₂, recognizing reaction barriers and rate-determining steps, and tracking intermediate formation pathways, in addition to considering factors like electrolyte pH and external bias, we can gain a deeper understanding of the CO₂ photocatalytic reduction process and the significance of catalysts.

The oxygen vacancy functions as an active site that may supply a lot of suspension bonds for the adsorption and activation of CO₂. In addition, these active sites can decrease the reaction energy barrier and increase the reaction rate. Even though much research has been done on how oxygen vacancies can improve photocatalytic CO₂ reduction, more

has to be learned about sophisticated synthesis techniques that can precisely control the position of oxygen vacancies. In addition, additional advancements in detecting technologies are required to precisely determine the concentration and location of oxygen vacancies in catalysts. Theoretical computations and in-situ spectroscopic characterization must be reinforced to thoroughly investigate the mechanism of photocatalytic CO₂ reduction on the catalyst with oxygen vacancy.

Plasmonic metals such as, Ag, Au, Pt, and Pd etc. have a significant effect on the CO₂ selectivity and photoactivity. Because of their exorbitant cost, plasmonic metals have not gotten as much attention in practical applications. Selecting the right cocatalyst is essential to fully comprehending this interaction mechanism.

Currently, powdered CeO₂-based photocatalysts are widely used. Unfortunately, the recovery and separation of these photocatalysts necessitate complex procedures such as centrifugation and drying. These processes can lead to substantial loss of photocatalysts and the potential for secondary pollution in the surrounding environment. Furthermore, thorough mixing is a critical experimental technique for dispersing the powder photocatalyst into the liquid solution. Nevertheless, this powerful mechanical mixing treatment often deviates from practical applications. Thus, to address the mentioned problem, exploring an innovative method for enhancing the state of photocatalysts is essential. Developing a macroscopic, three-dimensional (3D) aerogel photocatalyst using CeO₂ is a promising approach that requires further exploration.

Despite the competitive CO₂ conversion efficiency of the CeO₂ photocatalyst when compared to other commonly used photocatalysts. Optimizing the reactor's design parameters is crucial for achieving practical use and maximizing the efficient utilization of light and catalyst in the future.

Currently, most photocatalytic CO₂ reduction research is conducted in laboratories, far below levels of practical application. Significant barriers for researchers include issues with photostability, light absorption efficiency, material costs, and catalyst longevity. On the other hand, studying photocatalysts for CO₂ reduction is crucial for human growth from a societal standpoint. The initiative can potentially reduce environmental problems worldwide and pave the way for future creative energy solutions.

6. Conclusions

Efforts to combat global warming and address energy-related issues have increasingly focused on the solar-driven reduction of CO₂ into valuable fuels and substances. This process leverages the eco-friendly and economically viable nature of CO₂ photocatalytic reduction using sunlight-activated semiconductor materials. Despite notable progress, many solar-active catalysts for CO₂ photoreduction still face challenges, including low efficiency, uncontrollable selectivity, and instability. CeO₂, a commonly used semiconductor, exhibits limited sunlight absorption, necessitating modifications to enhance its performance in visible light. Various methods such as metal and non-metal doping, oxygen vacancy creation, and the addition of co-catalyst and nanocomposites production, including binary, ternary, Z-Scheme, and S-scheme heterostructures have been employed to improve CeO₂'s photoreactivity. These modifications have resulted in significant advancements in CO₂ conversion performance, with improving charge separation and light absorption and morphological changes enhancing overall efficiency. However, there remains a lack of comprehensive studies on the characteristics and precise photochemical reduction mechanisms of modified CeO₂. This review has aimed to bridge this gap by thoroughly examining recent breakthroughs in CeO₂-based photo reductants for CO₂ reduction. It has highlighted the mechanisms of CO₂ reduction into high-valued fuels, discussed methods involved in synthesizing photocatalysts, evaluated efficiency enhancement strategies, and explored the efficiencies and selectivity for reduction products. To further advance the field, this review also aims to provide invaluable

insights into the existing challenges and outline the future research opportunities on optimizing synthetic methods, understanding the rate-limiting steps through computational analysis, and exploring higher illumination intensities. Ultimately, a deeper understanding of the key variables impacting photocatalytic activity, stability, and selectivity will guide the development of more efficient and sustainable CO₂ reduction strategies.

CRediT authorship contribution statement

Kazi Arafin: Writing – review & editing, Writing – original draft.
Wahid Ullah: Writing – review & editing, Writing – original draft.
Hossain M. Shahadat: Writing – review & editing, Writing – original draft, Conceptualization.
Mohammad Sayadur Rahaman: Writing – review & editing, Writing – original draft, Supervision, Resources, Conceptualization.
Khondaker Afrina Hoque: Writing – review & editing, Writing – original draft, Methodology, Conceptualization.
Al-Nakib Chowdhury: Writing – review & editing, Writing – original draft, Supervision, Methodology, Funding acquisition, Formal analysis, Conceptualization.
Farjana Akter: Writing – review & editing, Writing – original draft.
Sharmin Ara Sathi: Writing – review & editing, Writing – original draft.
Tahsin Ahmed: Writing – review & editing, Writing – original draft.
Tania Akter: Writing – review & editing, Writing – original draft.

Declaration of Competing Interest

The authors certify that they have NO affiliations with or involvement in any organization or entity with any financial interest (such as honoraria; educational grants; participation in speakers' bureaus; membership, employment, consultancies, stock ownership, or other equity interest; and expert testimony or patent-licensing arrangements), or non-financial interest (such as personal or professional relationships, affiliations, knowledge or beliefs) in the subject matter or materials discussed in this manuscript.

Data Availability

Data will be made available on request.

References

- [1] A. Sharma, A. Hosseini-Bandegharaei, N. Kumar, S. Kumar, K. Kumari, Insight into ZnO/Carbon hybrid materials for photocatalytic reduction of CO₂: an in-depth review, *J. CO₂ Util.* 65 (2022) 102205, <https://doi.org/10.1016/j.jcou.2022.102205>.
- [2] Z.X. Bi, R.T. Guo, X. Hu, J. Wang, X. Chen, W.G. Pan, Research progress on photocatalytic reduction of CO₂ Based on LDH materials, *Nanoscale* 14 (9) (2022) 3367–3386, <https://doi.org/10.1039/d1nr08235c>.
- [3] S. Hussain, Y. Wang, L. Guo, T. He, Theoretical Insights into the mechanism of photocatalytic reduction of CO₂ over semiconductor catalysts, *J. Photochem. Photobiol. C: Photochem. Rev.* 52 (2022) 100538, <https://doi.org/10.1016/j.jphotochemrev.2022.100538>.
- [4] Y. Zhang, H. Liu, F. Gao, X. Tan, Y. Cai, B. Hu, Q. Huang, M. Fang, X. Wang, Application of MOFs and COFs for Photocatalysis in CO₂ Reduction, H₂ Generation, and Environmental Treatment, *EnergyChem* 4 (4) (2022) 100078, <https://doi.org/10.1016/j.enchem.2022.100078>.
- [5] L. Yuan, M. Qi, Z. Tang, Y. Xu, Coupling Strategy for CO₂ Valorization Integrated with Organic Synthesis by Heterogeneous Photocatalysis, *Angew. Chem. Int. Ed.* 60 (39) (2021) 21150–21172, <https://doi.org/10.1002/anie.202101667>.
- [6] Y. Shi, J. Li, C. Mao, S. Liu, X. Wang, X. Liu, S. Zhao, X. Liu, Y. Huang, L. Zhang, Van Der Waals Gap-Rich BiOCl Atomic Layers Realizing Efficient, Pure-Water CO₂-to-CO Photocatalysis, *Nat. Commun.* 12 (1) (2021) 5923, <https://doi.org/10.1038/s41467-021-26219-6>.
- [7] L. Jia, X. Tan, T. Yu, J. Ye, Mixed Metal Sulfides for the Application of Photocatalytic Energy Conversion, *Energy Fuels* 36 (19) (2022) 11308–11322, <https://doi.org/10.1021/acs.energyfuels.2c01137>.
- [8] Z. Ma, Y. Chen, C. Gao, Y. Xiong, A Minireview on the Role of Cocatalysts in Semiconductor-Based Photocatalytic CH₄ Conversion, *Energy Fuels* 36 (19) (2022) 11428–11442, <https://doi.org/10.1021/acs.energyfuels.2c01351>.
- [9] T. Suguro, F. Kishimoto, K. Takanabe, Photocatalytic Hydrogen Production under Water Vapor Feeding—A Minireview, *Energy Fuels* 36 (16) (2022) 8978–8994, <https://doi.org/10.1021/acs.energyfuels.2c01478>.
- [10] Z. wen Wang, Y. zhang Shi, C. Liu, Y. yue Kang, L. Wu, Cu+-Ti3+ Interface Interaction Mediated CO₂ Coordination Model for Controlling the Selectivity of Photocatalytic Reduction CO₂, *Appl. Catal. B* 301 (2022) 120803, <https://doi.org/10.1016/j.apcatb.2021.120803>.
- [11] Y. Zhou, Q. Zhang, X. Shi, Q. Song, C. Zhou, D. Jiang, Photocatalytic Reduction of CO₂ into CH₄ over Ru-Doped TiO₂: Synergy of Ru and Oxygen Vacancies, *J. Colloid Interface Sci.* 608 (2022) 2809–2819, <https://doi.org/10.1016/j.jcis.2021.11.011>.
- [12] R.G. Yang, Y.M. Fu, H.N. Wang, D.P. Zhang, Z. Zhou, Y.Z. Cheng, X. Meng, Y. O. He, Z.M. Su, ZIF-8/Covalent Organic Framework for Enhanced CO₂ Photocatalytic Reduction in Gas-Solid System, *Chem. Eng. J.* (2022) 450, <https://doi.org/10.1016/j.cej.2022.138040>.
- [13] Y. Zheng, Z. Duan, R. Liang, R. Lv, C. Wang, Z. Zhang, S. Wan, S. Wang, H. Xiong, C.K. Ngaw, J. Lin, Y. Wang, Shape-Dependent Performance of Cu/Cu₂O for Photocatalytic Reduction of CO₂, *ChemSusChem* 15 (10) (2022) 6–11, <https://doi.org/10.1002/cssc.202200216>.
- [14] H. Ou, S. Ning, P. Zhu, S. Chen, A. Han, Q. Kang, Z. Hu, J. Ye, D. Wang, Y. Li, Carbon Nitride Photocatalysts with Integrated Oxidation and Reduction Atomic Active Centers for Improved CO₂ Conversion, *Angew. Chem. Int. Ed. Engl.* 61 (34) (2022) e202206579, <https://doi.org/10.1002/anie.202206579>.
- [15] J. Shen, Z. Wu, C. Li, C. Zhang, A. Genest, G. Rupprecht, L. He, Emerging Applications of MXene Materials in CO₂ Photocatalysis, *FlatChem* 28 (2021) 100252, <https://doi.org/10.1016/j.flatc.2021.100252>.
- [16] L. Huang, D. Li, D. Tian, L. Jiang, Z. Li, H. Wang, K. Li, Optimization of Ni-Based Catalysts for Dry Reforming of Methane via Alloy Design: A Review, *Energy Fuels* 36 (10) (2022) 5102–5151, <https://doi.org/10.1021/acs.energyfuels.2c00523>.
- [17] L. Cheng, X. Yue, L. Wang, D. Zhang, P. Zhang, J. Fan, Q. Xiang, Dual-Single-Atom Tailoring with Bifunctional Integration for High-Performance CO₂ Photoreduction, *Adv. Mater.* 33 (49) (2021) 1–11, <https://doi.org/10.1002/adma.201405135>.
- [18] N.S. Lewis, D.G. Nocera, Powering the Planet: Chemical Challenges in Solar Energy Utilization, *Proc. Natl. Acad. Sci. USA* 103 (43) (2006) 15729–15735, <https://doi.org/10.1073/pnas.0603395103>.
- [19] S. Habisreutinger, L. Schmidt-Mende, J.K. Stolarczyk, Photocatalytic Reduction of CO₂ on TiO₂ and Other Semiconductors, *Angew. Chem. Int. Ed.* 52 (29) (2013) 7372–7408, <https://doi.org/10.1002/anie.201207199>.
- [20] S. Xie, Q. Zhang, G. Liu, Y. Wang, Photocatalytic and Photoelectrocatalytic Reduction of CO₂ Using Heterogeneous Catalysts with Controlled Nanostructures, *Chem. Commun.* 52 (1) (2016) 35–59, <https://doi.org/10.1039/C5CC07613G>.
- [21] B. Kumar, M. Llorente, J. Froehlich, T. Dang, A. Sathrum, C.P. Kubiak, Photochemical and Photoelectrochemical Reduction of CO₂, *Annu. Rev. Phys. Chem.* 63 (1) (2012) 541–569, <https://doi.org/10.1146/annurevophyschem-032511-143759>.
- [22] J. Hong, W. Zhang, J. Ren, R. Xu, Photocatalytic Reduction of CO₂: A Brief Review on Product Analysis and Systematic Methods, *Anal. Methods* 5 (5) (2013) 1086, <https://doi.org/10.1039/c2ay26270c>.
- [23] K. Kočí, H. Dang Van, M. Edelmannová, M. Reli, J.C.S. Wu, Photocatalytic Reduction of CO₂ Using Pt/C₃N₄ Photocatalysts, *Appl. Surf. Sci.* 503 (October 2019) (2020) 144426, <https://doi.org/10.1016/j.apsusc.2019.144426>.
- [24] Ali Hiragond, Sorcar, Hierarchical Nanostructured Photocatalysts for CO₂ Photoreduction, *Catalysts* 9 (4) (2019) 370, <https://doi.org/10.3390/catal9040370>.
- [25] A. Ziari, A. Badiei, R. Grillo, T. Burgi, 3D Yolk@Shell TiO_{2-x}/LDH Architecture: Tailored Structure for Visible Light CO₂ Conversion, *ACS Appl. Mater. Interfaces* 11 (6) (2019) 5903–5910, <https://doi.org/10.1021/acsami.8b17232>.
- [26] G. Yergaziyeva, Z. Kuspanov, M. Mamchetova, N. Khudaibergenov, N. Makayeva, C. Daubayev, Advancements in Catalytic, Photocatalytic, and Electrocatalytic CO₂ Conversion Processes: Current Trends and Future Outlook, *J. CO₂ Util.* 80 (2024) 102682, <https://doi.org/10.1016/j.jcou.2024.102682>.
- [27] X. Li, J. Wen, J. Low, Y. Fang, J. Yu, Design and Fabrication of Semiconductor Photocatalyst for Photocatalytic Reduction of CO₂ to Solar Fuel, *Sci. China Mater.* 57 (1) (2014) 70–100, <https://doi.org/10.1007/s40843-014-0003-1>.
- [28] W. Tu, Y. Zhou, Z. Zou, Photocatalytic Conversion of CO₂ into Renewable Hydrocarbon Fuels: State-of-the-Art Accomplishment, Challenges, and Prospects, *Adv. Mater.* 26 (27) (2014) 4607–4626, <https://doi.org/10.1002/adma.201400087>.
- [29] R. Zhao, L. Huan, P. Gu, R. Guo, M. Chen, G. Diao, Yb,Er-Doped CeO₂ Nanotubes as an Assistant Layer for Photoconversion-Enhanced Dye-Sensitized Solar Cells, *J. Power Sources* 331 (2016) 527–534, <https://doi.org/10.1016/j.jpowsour.2016.09.039>.
- [30] L. Guan, S. Le, S. He, X. Zhu, T. Liu, K. Sun, Densification Behavior and Space Charge Blocking Effect of Bi₂O₃ and Gd₂O₃ Co-Doped CeO₂ as Electrolyte for Solid Oxide Fuel Cells, *Electrochimica Acta* 161 (2015) 129–136, <https://doi.org/10.1016/j.electacta.2015.02.090>.
- [31] J. Liu, M. Dai, T. Wang, P. Sun, X. Liang, G. Lu, K. Shimano, N. Yamazoe, Enhanced Gas Sensing Properties of SnO₂ Hollow Spheres Decorated with CeO₂ Nanoparticles Heterostructure Composite Materials, *ACS Appl. Mater. Interfaces* 8 (10) (2016) 6669–6677, <https://doi.org/10.1021/acsami.6b00169>.
- [32] D.P.H. Tran, M.T. Pham, X.T. Bui, Y.F. Wang, S.J. You, CeO₂ as a Photocatalytic Material for CO₂ Conversion: A Review, *Sol. Energy* (2022) 443–466, <https://doi.org/10.1016/j.solener.2022.04.051>.

- [33] J. Gong, F. Meng, X. Yang, Z. Fan, H. Li, Controlled Hydrothermal Synthesis of Triangular CeO₂ Nanosheets and Their Formation Mechanism and Optical Properties, *J. Alloy. Compd.* 689 (2016) 606–616, <https://doi.org/10.1016/j.jallcom.2016.08.030>.
- [34] R. Fiorenza, M. Bellardita, S.A. Balsamo, L. Spitaleri, A. Gulino, M. Condorelli, L. D’Urso, S. Scirè, L. Palmisano, A Solar Photothermocatalytic Approach for the CO₂ Conversion: Investigation of Different Synergisms on CoO-CuO/Brookite TiO₂-CeO₂ Catalysts, *Chem. Eng. J.* (2022) 428, <https://doi.org/10.1016/j.cej.2021.131249>.
- [35] M. Tahir, N.A.S. Amin, Photo-Induced CO₂ Reduction by Hydrogen for Selective CO Evolution in a Dynamic Monolith Photoreactor Loaded with Ag-Modified TiO₂ Nanocatalyst, *Int. J. Hydrom. Energy* 42 (23) (2017) 15507–15522, <https://doi.org/10.1016/j.ijhydene.2017.05.039>.
- [36] A. Ali, M.R.U.D. Biswas, W.C. Oh, Novel and Simple Process for the Photocatalytic Reduction of CO₂ with Ternary Bi2O₃-Graphene-ZnO Nanocomposite, *J. Mater. Sci.: Mater. Electron.* 29 (12) (2018) 10222–10233, <https://doi.org/10.1007/s10854-018-9073-5>.
- [37] N. Nie, L. Zhang, J. Fu, B. Cheng, J. Yu, Self-Assembled Hierarchical Direct Z-Scheme g-C₃N₄/ZnO Microspheres with Enhanced Photocatalytic CO₂ Reduction Performance, *Appl. Surf. Sci.* 441 (2018) 12–22, <https://doi.org/10.1016/j.apusc.2018.01.193>.
- [38] J. Li, F. Wei, C. Dong, W. Mu, X. Han, A Z-Scheme ZnFe2O4/RGO/In2O3 Hierarchical Photocatalyst for Efficient CO₂ Reduction Enhancement, *J. Mater. Chem. A Mater.* 8 (14) (2020) 6524–6531, <https://doi.org/10.1039/c9ta13774b>.
- [39] X. Chen, Y. Huang, H. Li, Y. Li, X. Wang, X. Zhu, X. Xu, Assessment of CO₂ Photoconversion over TiO₂/La₂O₃ Treated with Acetic Acid, *Mater. Lett.* (2021) 303, <https://doi.org/10.1016/j.matlet.2021.130466>.
- [40] A. Raza, H. Shen, A.A. Haidry, L. Sun, R. Liu, S. Cui, Studies of Z-Scheme WO₃-TiO₂/Cu₂ZnSnS₄ Ternary Nanocomposite with Enhanced CO₂ Photoreduction under Visible Light Irradiation, *J. CO₂ Util.* 37 (2020) 260–271, <https://doi.org/10.1016/j.jcou.2019.12.020>.
- [41] Z. Wang, K. Teramura, S. Hosokawa, T. Tanaka, Photocatalytic Conversion of CO₂ in Water over Ag-Modified La₂Ti₂O₇, *Appl. Catal. B* 163 (2015) 241–247, <https://doi.org/10.1016/j.apcatb.2014.07.052>.
- [42] M. Tahir, A. Ali Khan, S. Tasleem, R. Mansoor, W.K. Fan, Titanium Carbide (Ti₃C₂) MXene as a Promising Co-Catalyst for Photocatalytic CO₂Conversion to Energy-Efficient Fuels: A Review, *Energy Fuels* (2021) 10374–10404, <https://doi.org/10.1021/acs.energyfuels.1c00958>.
- [43] H. Lai, X. Zeng, T. Song, S. Yin, B. Long, A. Ali, G.J. Deng, Fast Synthesis of Porous Iron Doped CeO₂ with Oxygen Vacancy for Effective CO₂ Photoreduction, *J. Colloid Interface Sci.* 608 (2022) 1792–1801, <https://doi.org/10.1016/j.jcis.2021.10.064>.
- [44] M. Aslam, M.T. Qamar, M.T. Soomro, I.M.I. Ismail, N. Salah, T. Almeelbi, M. A. Gondal, A. Hameed, The Effect of Sunlight Induced Surface Defects on the Photocatalytic Activity of Nanosized CeO₂ for the Degradation of Phenol and Its Derivatives, *Appl. Catal. B* 180 (2016) 391–402, <https://doi.org/10.1016/j.apcatb.2015.06.050>.
- [45] J. Cai, D. Li, L. Jiang, J. Yuan, Z. Li, K. Li, Review on CeO₂ -Based Photocatalysts for Photocatalytic Reduction of CO₂: Progresses and Perspectives, *Energy Fuels* 37 (7) (2023) 4878–4897, <https://doi.org/10.1021/acs.energyfuels.3c0120>.
- [46] J.L. White, M.F. Baruch, J.E. Pander, Y. Hu, I.C. Fortmeyer, J.E. Park, T. Zhang, K. Liao, J. Gu, Y. Yan, T.W. Shaw, E. Abelev, A.B. Bocarsly, Light-Driven Heterogeneous Reduction of Carbon Dioxide: Photocatalysts and Photoelectrodes, *Chem. Rev.* 115 (23) (2015) 12888–12935, <https://doi.org/10.1021/acs.chemrev.5b00370>.
- [47] X. Chang, T. Wang, J. Gong, CO₂ Photo-Reduction: Insights into CO₂ Activation and Reaction on Surfaces of Photocatalysts, *Energy Environ. Sci.* 9 (7) (2016) 2177–2196, <https://doi.org/10.1039/c6ee00383d>.
- [48] A.O. Adeola, J.O. Igahlo, P.I. Kyesmen, P.N. Nomngongo, Metal-Organic Polyhedra (MOPs) as Emerging Class of Metal-Organic Frameworks for CO₂ Photocatalytic Conversions: Current Trends and Future Outlook, *J. CO₂ Util.* 80 (2024) 102664, <https://doi.org/10.1016/j.jcou.2023.102664>.
- [49] Q. Mou, Z. Guo, Y. Chai, B. Liu, C. Liu, Visible Light Assisted Production of Methanol from CO₂ Using CdS@CeO₂ Heterojunction, *J. Photochem. Photobio. B* 219 (2021) 112205, <https://doi.org/10.1016/j.jphotobiol.2021.112205>.
- [50] H. Song, R. Wu, Y. Yang, J. Dong, G. Ji, Fabrication of CeO₂ Nanoparticles Decorated Three-Dimensional Flower-like BiOI Composites to Build p-n Heterojunction with Highly Enhanced Visible-Light Photocatalytic Performance, *J. Colloid Interface Sci.* 512 (2018) 325–334, <https://doi.org/10.1016/j.jcis.2017.10.080>.
- [51] X.J. Wen, C.G. Niu, L. Zhang, C. Liang, G.M. Zeng, A Novel Ag₂O/CeO₂ Heterojunction Photocatalysts for Photocatalytic Degradation of Enrofloxacin: Possible Degradation Pathways, Mineralization Activity and an in Depth Mechanism Insight, *Appl. Catal. B* 221 (2018) 701–714, <https://doi.org/10.1016/j.apcatb.2017.09.060>.
- [52] X.J. Wen, C. Zhang, C.G. Niu, L. Zhang, G.M. Zeng, X.G. Zhang, Highly Enhanced Visible Light Photocatalytic Activity of CeO₂ through Fabricating a Novel p-n Junction BiOBr/CeO₂, *Catal. Commun.* 90 (2017) 51–55, <https://doi.org/10.1016/j.catcom.2016.11.018>.
- [53] D. Channei, B. Inceesungvorn, N. Wetchakun, S. Ukrithunkun, A. Nattestad, J. Chen, S. Phanichphant, Photocatalytic Degradation of Methyl Orange by CeO₂ and Fe-Doped CeO₂ Films under Visible Light Irradiation, *Sci. Rep.* 4 (1) (2014) 5757, <https://doi.org/10.1038/srep05757>.
- [54] D. Tomova, V. Iliev, A. Eliyas, S. Rakovsky, Promoting the Oxidative Removal Rate of Oxalic Acid on Gold-Doped CeO₂/TiO₂ Photocatalysts under UV and Visible Light Irradiation, *Sep Purif. Technol.* 156 (2015) 715–723, <https://doi.org/10.1016/j.seppur.2015.10.070>.
- [55] W. Lei, T. Zhang, L. Gu, P. Liu, J.A. Rodriguez, G. Liu, M. Liu, Surface-Structure Sensitivity of CeO₂ Nanocrystals in Photocatalysis and Enhancing the Reactivity with Nanogold, *ACS Catal.* 5 (7) (2015) 4385–4393, <https://doi.org/10.1021/acscatal.5b00620>.
- [56] Z. Fan, F. Meng, J. Gong, H. Li, Y. Hu, D. Liu, Enhanced Photocatalytic Activity of Hierarchical Flower-like CeO₂/TiO₂ Heterostructures, *Mater. Lett.* 175 (2016) 36–39, <https://doi.org/10.1016/j.matlet.2016.03.136>.
- [57] K. Li, C. Teng, S. Wang, Q. Min, Recent Advances in TiO₂-Based Heterojunctions for Photocatalytic CO₂ Reduction With Water Oxidation: A Review, *Front Chem.* 9 (2021) 1–25, <https://doi.org/10.3389/fchem.2021.637501>.
- [58] Y. Gao, K. Qian, B. Xu, Z. Li, J. Zheng, S. Zhao, F. Ding, Y. Sun, Z. Xu, Recent Advances in Visible-Light-Driven Conversion of CO₂ by Photocatalysts into Fuels or Value-Added Chemicals, *Carbon Resour. Convers.* 3 (2020) 46–59, <https://doi.org/10.1016/j.crcn.2020.02.003>.
- [59] T.P. Nguyen, D.L.T. Nguyen, V.-H. Nguyen, T.-H. Le, D.-V.N. Vo, Q.T. Trinh, S.-R. Bae, S.Y. Chae, S.Y. Kim, Q.Van Le, Recent Advances in TiO₂-Based Photocatalysts for Reduction of CO₂ to Fuels, *Nanomaterials* 10 (2) (2020) 337, <https://doi.org/10.3390/nano10020337>.
- [60] Y. Wang, F. Wang, Y. Chen, D. Zhang, B. Li, S. Kang, X. Li, L. Cui, Enhanced Photocatalytic Performance of Ordered Mesoporous Fe-Doped CeO₂ Catalysts for the Reduction of CO₂ with H₂O under Simulated Solar Irradiation, *Appl. Catal. B* 147 (2014) 602–609, <https://doi.org/10.1016/j.apcatb.2013.09.036>.
- [61] Z.-L. Wang, G.-R. Li, Y.-N. Ou, Z.-P. Feng, D.-L. Qu, Y.-X. Tong, Electrochemical Deposition of Eu³⁺-Doped CeO₂ Nanobelts with Enhanced Optical Properties, *J. Phys. Chem. C* 115 (2) (2011) 351–356, <https://doi.org/10.1021/jp1070924>.
- [62] Y. Wang, X. Bai, F. Wang, S. Kang, C. Yin, X. Li, Nanocasting Synthesis of Chromium Doped Mesoporous CeO₂ with Enhanced Visible-Light Photocatalytic CO₂ Reduction Performance, *J. Hazard. Mater.* 372 (2019) 69–76, <https://doi.org/10.1016/j.jhazmat.2017.10.007>.
- [63] M. Wang, M. Shen, X. Jin, J. Tian, Y. Shao, L. Zhang, Y. Li, J. Shi, Exploring the Enhancement Effects of Hetero-Metal Doping in CeO₂ on CO₂ Photocatalytic Reduction Performance, *Chem. Eng. J.* 427 (2022) 130987, <https://doi.org/10.1016/j.cej.2021.130987>.
- [64] L. Li, P. Li, Y. Wang, L. Lin, A.H. Shah, T. He, Modulation of Oxygen Vacancy in Hydrangea-like Ceria via Zr Doping for CO₂ Photoreduction, *Appl. Surf. Sci.* 452 (2018) 498–506, <https://doi.org/10.1016/j.apusc.2018.04.256>.
- [65] L. Jiang, X. Yuan, Y. Pan, J. Liang, G. Zeng, Z. Wu, H. Wang, Doping of Graphitic Carbon Nitride for Photocatalysis: A Review, *Appl. Catal. B* 217 (2017) 388–406, <https://doi.org/10.1016/j.apcatb.2017.06.003>.
- [66] M. Samadi, M. Zirak, A. Nasiri, E. Khorashadizade, A.Z. Moshfegh, Recent Progress on Doped ZnO Nanostructures for Visible-Light Photocatalysis, *Thin Solid Films* 605 (2016) 2–19, <https://doi.org/10.1016/j.tsf.2015.12.064>.
- [67] S.J. Shi, S.S. Zhou, S.Q. Liu, Z.G. Chen, Photocatalytic Activity of Erbium-Doped CeO₂ Enhanced by Reduced Graphene Oxide/CuO Cocatalyst for the Reduction of CO₂ to Methanol, *Environ. Prog. Sustain. Energy* 37 (2) (2018) 655–662, <https://doi.org/10.1002/ep.12717>.
- [68] H. Zhang, Y. Liao, G. Yang, X. Zhou, Theoretical Studies on the Electronic and Optical Properties of Honeycomb BC 3 Monolayer: A Promising Candidate for Metal-Free Photocatalysts, *ACS Omega* 3 (9) (2018) 10517–10525, <https://doi.org/10.1021/acsomega.8b01998>.
- [69] C. Yu, L. Wei, J. Chen, Y. Xie, W. Zhou, Q. Fan, Enhancing the Photocatalytic Performance of Commercial TiO₂ Crystals by Coupling with Trace Narrow-Band-Gap Ag₂CO₃, *Ind. Eng. Chem. Res.* 53 (14) (2014) 5759–5766, <https://doi.org/10.1021/ie404283d>.
- [70] M. Ni, M.K.H. Leung, D.Y.C. Leung, K. Sumathy, A Review and Recent Developments in Photocatalytic Water-Splitting Using TiO₂ for Hydrogen Production, *Renew. Sustain. Energy Rev.* 11 (3) (2007) 401–425, <https://doi.org/10.1016/j.rser.2005.01.009>.
- [71] Q. Wang, Y. Chen, X. Liu, L. Li, L. Du, G. Tian, Sulfur Doped In2O3-CeO₂ Hollow Hexagonal Prisms with Carbon Coating for Efficient Photocatalytic CO₂ Reduction, *Chem. Eng. J.* 421 (P1) (2021) 129968, <https://doi.org/10.1016/j.cej.2021.129968>.
- [72] B. Choudhury, P. Chetri, A. Choudhury, Oxygen Defects and Formation of Ce³⁺ Affecting the Photocatalytic Performance of CeO₂ Nanoparticles, *RSC Adv.* 4 (9) (2014) 4663–4671, <https://doi.org/10.1039/C3RA44603D>.
- [73] L. Yan, R. Yu, J. Chen, X. Xing, Template-Free Hydrothermal Synthesis of CeO₂ Nano-Octahedrons and Nanorods: Investigation of the Morphology Evolution, *Cryst. Growth Des.* 8 (5) (2008) 1474–1477, <https://doi.org/10.1021/cg800117v>.
- [74] A. Hezam, K. Namratha, Q.A. Drmosh, D. Ponnamma, J. Wang, S. Prasad, M. Ahamed, C. Cheng, K. Byrappa, CeO₂ Nanostructures Enriched with Oxygen Vacancies for Photocatalytic CO₂ Reduction, *ACS Appl. Nano Mater.* 3 (1) (2020) 138–148, <https://doi.org/10.1021/acsanm.9b01833>.
- [75] M. Wang, M. Shen, X. Jin, J. Tian, M. Li, Y. Zhou, L. Zhang, Y. Li, J. Shi, Oxygen Vacancy Generation and Stabilization in CeO₂–x by Cu Introduction with Improved CO₂ Photocatalytic Reduction Activity, *ACS Catal.* 9 (5) (2019) 4573–4581, <https://doi.org/10.1021/acscatal.8b03975>.
- [76] M. Wang, M. Shen, X. Jin, J. Tian, Y. Zhou, Y. Shao, L. Zhang, Y. Li, J. Shi, Mild Generation of Surface Oxygen Vacancies on CeO₂ for Improved CO₂ Photoreduction Activity, *Nanoscale* 12 (23) (2020) 12374–12382, <https://doi.org/10.1039/donr00717j>.
- [77] W. Li, S. Ma, G. Yang, Y. Mao, J. Luo, L. Cheng, D. Gengzhang, X. Xu, S. Yan, Preparation, Characterization and Gas Sensing Properties of Pure and Ce Doped

- ZnO Hollow Nanofibers, *Mater. Lett.* **138** (36) (2015) 188–191, <https://doi.org/10.1016/j.matlet.2014.09.130>.
- [78] R. Lamba, A. Umar, S.K. Mehta, S.K. Kansal, CeO₂ZnO Hexagonal Nanodisks: Efficient Material for the Degradation of Direct Blue 15 Dye and Its Simulated Dye Bath Effluent under Solar Light, *J. Alloy. Compd.* **620** (2015) 67–73, <https://doi.org/10.1016/j.jallcom.2014.09.101>.
- [79] T. Ye, W. Huang, L. Zeng, M. Li, J. Shi, CeO₂-x Platelet from Monometallic Cerium Layered Double Hydroxides and Its Photocatalytic Reduction of, *Appl. Catal. B* **210** (141–148) (2017) CO2, <https://doi.org/10.1016/j.apcatb.2017.03.051>.
- [80] J. Kašpar, P. Fornasiero, M. Graziani, Use of CeO₂-Based Oxides in the Three-Way Catalysis, *Catal. Today* **50** (2) (1999) 285–298, [https://doi.org/10.1016/S0920-5861\(98\)00510-0](https://doi.org/10.1016/S0920-5861(98)00510-0).
- [81] J. Zheng, Z. Zhu, G. Gao, Z. Liu, Q. Wang, Y. Yan, Construction of Spindle Structured CeO₂ Modified with Rod-like Attapulgite as a High-Performance Photocatalyst for CO₂ Reduction, *Catal. Sci. Technol.* **9** (14) (2019) 3788–3799, <https://doi.org/10.1039/C9CY00824A>.
- [82] V. Golovanova, M.C. Spadaro, J. Arbiol, V. Golovanov, T.T. Rantala, T. Andreu, J.R. Morante, Effects of Solar Irradiation on Thermally Driven CO₂ Methanation Using Ni/CeO₂-Based Catalyst, *Appl. Catal. B* **291** (2021) 120038, <https://doi.org/10.1016/j.apcatb.2021.120038>.
- [83] H. Jiang, X. Li, S. Chen, H. Wang, P. Huo, G-C3N4 Quantum Dots-Modified Mesoporous CeO₂ Composite Photocatalyst for Enhanced CO₂ Photoreduction, *J. Mater. Sci.: Mater. Electron.* **31** (22) (2020) 20495–20512, <https://doi.org/10.1007/s10854-020-04568-0>.
- [84] S.-S. Zhou, S.-Q. Liu, Photocatalytic Reduction of CO₂ Based on a CeO₂ Photocatalyst Loaded with Imidazole Fabricated N-Doped Graphene and Cu(II) as Cocatalysts, *Photochem. Photobiol. Sci.* **16** (10) (2017) 1563–1569, <https://doi.org/10.1039/c7pp00211d>.
- [85] S. Dong, J. Feng, M. Fan, Y. Pi, L. Hu, X. Han, M. Liu, J. Sun, Recent Developments in Heterogeneous Photocatalytic Water Treatment Using Visible Light-Responsive Photocatalysts: A Review, *RSC Adv.* **5** (19) (2015) 14610–14630, <https://doi.org/10.1039/C4RA13734E>.
- [86] W. Han, C. Zang, Z. Huang, H. Zhang, L. Ren, X. Qi, J. Zhong, Enhanced Photocatalytic Activities of Three-Dimensional Graphene-Based Aerogel Embedding TiO₂ Nanoparticles and Loading MoS₂ Nanosheets as Co-Catalyst, *Int. J. Hydrom. Energy* **39** (34) (2014) 19502–19512, <https://doi.org/10.1016/j.ijhydene.2014.09.043>.
- [87] S. Ijaz, M.F. Ehsan, M.N. Ashiq, N. Karamat, T. He, Preparation of CdS@CeO₂ Core/Shell Composite for Photocatalytic Reduction of CO₂ under Visible-Light Irradiation, *Appl. Surf. Sci.* **390** (2016) 550–559, <https://doi.org/10.1016/j.apsusc.2016.08.098>.
- [88] M. Li, L. Zhang, M. Wu, Y. Du, X. Fan, M. Wang, L. Zhang, Q. Kong, J. Shi, Mesostructured CeO₂/g-C3N4 Nanocomposites: Remarkably Enhanced Photocatalytic Activity for CO₂ Reduction by Mutual Component Activations, *Nano Energy* **19** (2016) 145–155, <https://doi.org/10.1016/j.nanoen.2015.11.010>.
- [89] H. Wang, J. Guan, J. Li, X. Li, C. Ma, P. Huo, Y. Yan, Fabricated G-C3N4/Ag/m-CeO₂ Composite Photocatalyst for Enhanced Photoconversion of CO₂, *Appl. Surf. Sci.* **506** (2020) 144931, <https://doi.org/10.1016/j.apsusc.2019.144931>.
- [90] Y. Wei, X. Li, Y. Zhang, Y. Yan, P. Huo, H. Wang, G-C3N4 Quantum Dots and Au Nano Particles Co-Modified CeO₂/Fe3O4 Micro-Flowers Photocatalyst for Enhanced CO₂ Photoreduction, *Renew. Energy* **179** (2021) 756–765, <https://doi.org/10.1016/j.renene.2021.07.091>.
- [91] Y. Wang, B. Li, C. Zhang, L. Cui, S. Kang, X. Li, L. Zhou, Ordered Mesoporous CeO₂-TiO₂ Composites: Highly Efficient Photocatalysts for the Reduction of CO₂ with H₂O under Simulated Solar Irradiation, *Appl. Catal. B* **130–131** (2013) 277–284, <https://doi.org/10.1016/j.apcatb.2012.11.019>.
- [92] W. Dai, X. Hu, T. Wang, W. Xiong, X. Luo, J. Zou, Hierarchical CeO₂/Bi₂MoO₆ Heterostructured Nanocomposites for Photoreduction of CO₂ into Hydrocarbons under Visible Light Irradiation, *Appl. Surf. Sci.* **434** (2018) 481–491, <https://doi.org/10.1016/j.apsusc.2017.10.207>.
- [93] J. Guan, H. Wang, J. Li, C. Ma, P. Huo, Enhanced Photocatalytic Reduction of CO₂ by Fabricating In2O3/CeO₂/HATP Hybrid Multi-Junction Photocatalyst, *J. Taiwan Inst. Chem. Eng.* **99** (2019) 93–103, <https://doi.org/10.1016/j.jtice.2019.03.007>.
- [94] Z. Xiong, Z. Lei, Z. Xu, X. Chen, B. Gong, Y. Zhao, H. Zhao, J. Zhang, C. Zheng, Flame Spray Pyrolysis Synthesized ZnO/CeO₂ Nanocomposites for Enhanced CO₂ Photocatalytic Reduction under UV-Vis Light Irradiation, *J. CO₂ Util.* **18** (2017) 53–61, <https://doi.org/10.1016/j.jcou.2017.01.013>.
- [95] P. Seeharaj, P. Kongmun, P. Paiplod, S. Prakobmit, C. Sriwong, P. Kim-Lohsoontorn, N. Vittayakorn, Ultrasonically-Assisted Surface Modified TiO₂/RGO/CeO₂ Heterojunction Photocatalysts for Conversion of CO₂ to Methanol and Ethanol, *Ultrason. Sonochem.* (2019) 58, <https://doi.org/10.1016/j.ulsonch.2019.104657>.
- [96] P.K. Prajapati, A. Malik, N. Nandal, S. Pandita, R. Singh, S. Bhandari, S. Saran, S. L. Jain, Morphology Controlled Fe and Ni-Doped CeO₂ Nanorods as an Excellent Heterojunction Photocatalyst for CO₂ Reduction, *Appl. Surf. Sci.* (2022) 588, <https://doi.org/10.1016/j.apsusc.2022.152912>.
- [97] Z. Pan, E. Han, J. Zheng, J. Lu, X. Wang, Y. Yin, G.J.N. Waterhouse, X. Wang, P. Li, Highly Efficient Photoelectrocatalytic Reduction of CO₂ to Methanol by a p-n Heterojunction CeO₂/CuO/Cu Catalyst, *Nanomicro Lett.* **12** (1) (2020) 18, <https://doi.org/10.1007/s40820-019-0354-1>.
- [98] M.M.M. Mostafa, A. Shawky, S.F. Zaman, K. Narasimharao, M. Abdel Salam, A. A. Alshehri, N.H. Khiday, S. Al-Faifi, A.D. Chowdhury, Visible-Light-Driven CO₂ Reduction into Methanol Utilizing Sol-Gel-Prepared CeO₂-Coupled Bi2O3 Nanocomposite Heterojunctions, *Catalysts* **12** (11) (2022) 1479, <https://doi.org/10.3390/catal12111479>.
- [99] M.A. Raza, W. Cai, H. Tian, M. Que, L. Zhu, X. Chen, Hierarchical Flower-like Ternary Composite of NiFeCr/PCN/CeO₂ towards Efficient Photocatalytic Reduction of CO₂, *J. Phys. Chem. Solids* **171** (2022) 111027, <https://doi.org/10.1016/j.jpcs.2022.111027>.
- [100] P.K. Prajapati, D. Garg, A. Malik, D. Kumar, V. Amoli, S.L. Jain, A Novel Ternary Metal Oxide Cascade Z-Scheme Heterojunction for Efficient CO₂photoconversion without a Co-Catalyst, *J. Environ. Chem. Eng.* **10** (4) (2022), <https://doi.org/10.1016/j.jece.2022.108147>.
- [101] Y.X. Feng, G.X. Dong, K. Su, Z.L. Liu, W. Zhang, M. Zhang, T.B. Lu, Self-Template-Oriented Synthesis of Lead-Free Perovskite Cs₃Bi₂I₉ Nanosheets for Boosting Photocatalysis of CO₂ Reduction over Z-Scheme Heterojunction Cs₃Bi₂I₉/CeO₂, *J. Energy Chem.* **69** (2022) 348–355, <https://doi.org/10.1016/j.jec.2022.01.015>.
- [102] H. Zhou, Y. Wang, J. Wu, W. Zhou, Y. Qi, Q. Liu, W. Kong, A. Hosseini-Bandegharaei, L. Ma, T. Guan, Enhanced Photocatalytic Reduction of CO₂ Using a Novel 2D/0D Sn₂/CeO₂ Binary Photocatalyst with Z-Scheme Heterojunction and Oxygen Vacancy, *J. CO₂ Util.* **76** (2023) 102591, <https://doi.org/10.1016/j.jcou.2023.102591>.
- [103] W. Li, L. Jin, F. Gao, H. Wan, Y. Pu, X. Wei, C. Chen, W. Zou, C. Zhu, L. Dong, Advantageous Roles of Phosphate Decorated Octahedral CeO₂ {111}/g-C3N4 in Boosting Photocatalytic CO₂ Reduction: Charge Transfer Bridge and Lewis Basic Site, *Appl. Catal. B* (2021) 294, <https://doi.org/10.1016/j.apcatb.2021.120257>.
- [104] S.A. Mahyoub, A. Hezam, F.A. Qarah, K. Namratha, M.B. Nayani, Q.A. Drmash, D. Ponnamma, K. Byrappa, Surface Plasmonic Resonance and Z-Scheme Charge Transport Synergy in Three-Dimensional Flower-like Ag-CeO₂–ZnO Heterostructures for Highly Improved Photocatalytic CO₂ Reduction, *ACS Appl. Energy Mater.* **4** (4) (2021) 3544–3554, <https://doi.org/10.1021/acsaem.1c00001>.
- [105] X. Li, J. Guan, H. Jiang, X. Song, P. Huo, H. Wang, RGO Modified R-CeO₂/g-C3N4 Multi-Interface Contact S-Scheme Photocatalyst for Efficient CO₂ Photoreduction, *Appl. Surf. Sci.* **563** (December 2020) (2021) 150042, <https://doi.org/10.1016/j.apsusc.2021.150042>.
- [106] Q. Zhu, N. Liu, Q. Ma, A. Sharma, D. Nagai, X. Sun, C. Zhang, Y. Yang, Sol-Gel/Hydrothermal Two-Step Synthesis Strategy for Promoting Ag Species-Modified TiO₂-Based Composite Activity toward H₂ Evolution under Solar Light, *Mater Today, Energy* (2021) 20, <https://doi.org/10.1016/j.mtener.2021.100648>.
- [107] Y.Q. Yan, Y.Z. Wu, Y.H. Wu, Z.L. Weng, S.J. Liu, Z.G. Liu, K.Q. Lu, B. Han, Recent Advances of CeO₂-Based Composite Materials for Photocatalytic Applications, *ChemSusChem*, John Wiley and Sons Inc, 2024, <https://doi.org/10.1002/cssc.202301778>.
- [108] M.A. Salaev, A.A. Salaeva, T.S. Kharlamova, G.V. Mamontov, Pt-CeO₂-Based Composites in Environmental Catalysis: A Review, *Appl. Catal. B* **295** (2021) 120286, <https://doi.org/10.1016/j.apcatb.2021.120286>.
- [109] R. Ma, S. Zhang, T. Wen, P. Gu, L. Li, G. Zhao, F. Niu, Q. Huang, Z. Tang, X. Wang, A Critical Review on Visible-Light-Response CeO₂-Based Photocatalysts with Enhanced Photooxidation of Organic Pollutants, *Catal. Today* **335** (2019) 20–30, <https://doi.org/10.1016/j.cattod.2018.11.016>.
- [110] F. Caddeo, D. Loche, M.F. Casula, A. Corrias, Growing CeO₂ Nanoparticles Within the Nano-Porous Architecture of the SiO₂ Aerogel, *Front Chem.* (2020) 8, <https://doi.org/10.3389/fchem.2020.00057>.
- [111] Z.U. Rehman, M. Bilal, J. Hou, F.K. Butt, J. Ahmad, S. Ali, A. Hussain, Photocatalytic CO₂ Reduction Using TiO₂-Based Photocatalysts and TiO₂ Z-Scheme Heterojunction Composites: A Review, *Molecules* (2022), <https://doi.org/10.3390/molecules27072069>.
- [112] N. Shehzad, M. Tahir, K. Johari, T. Murugesan, M. Hussain, A Critical Review on TiO₂ Based Photocatalytic CO₂ Reduction System: Strategies to Improve Efficiency, *J. CO₂ Util.* (2018) 98–122, <https://doi.org/10.1016/j.jcou.2018.04.026>.
- [113] Z. Shen, Q. Xia, Y. Li, C. Yin, Z. Ge, X. Li, Y. Wang, Adsorption-Enhanced Nitrogen-Doped Mesoporous CeO₂as an Efficient Visible-Light-Driven Catalyst for CO₂photoreduction, *J. CO₂ Util.* (2020) 39, <https://doi.org/10.1016/j.jcou.2020.101176>.
- [114] J. Albero, Y. Peng, H. Garcia, Photocatalytic CO₂Reduction to C₂+ Products, *ACS Catal.* **10** (2020) 5734–5749, <https://doi.org/10.1021/acscatal.0c00478>.
- [115] M. Liang, T. Borjigin, Y. Zhang, B. Liu, H. Liu, H. Guo, Controlled Assemble of Hollow Heterostructured G-C3N4@CeO₂ with Rich Oxygen Vacancies for Enhanced Photocatalytic CO₂ Reduction, *Appl. Catal. B* **243** (2019) 566–575, <https://doi.org/10.1016/j.apcatb.2018.11.010>.
- [116] X. Ren, M. Gao, Y. Zhang, Z. Zhang, X. Cao, B. Wang, X. Wang, Photocatalytic Reduction of CO₂ on BiO_x : Effect of Halogen Element Type and Surface Oxygen Vacancy Mediated Mechanism, *Appl. Catal. B* (2020) 274, <https://doi.org/10.1016/j.apcatb.2020.119063>.
- [117] X. Hu, Z. Xie, Q. Tang, H. Wang, L. Zhang, J. Wang, Enhanced CH₄ Yields by Interfacial Heating-Induced Hot Water Steam during Photocatalytic CO₂ Reduction, *Appl. Catal. B* (2021) 298, <https://doi.org/10.1016/j.apcatb.2021.120635>.
- [118] M. Compagnoni, G. Ramis, F.S. Freyria, M. Armandi, B. Bonelli, I. Rossetti, Innovative Photoreactors for Unconventional Photocatalytic Processes: The Photoreduction of CO₂ and the Photo-Oxidation of Ammonia, *Rend. Lincei--* **28** (2017) 151–158, <https://doi.org/10.1007/s12210-017-0617-z>.
- [119] H. Kawanami, D.C. Grills, T. Ishizaka, M. Chatterjee, A. Suzuki, Photocatalytic Reduction of CO₂ under Supercritical CO₂ Conditions: Effect of Pressure, Temperature, and Solvent on Catalytic Efficiency, *J. CO₂ Util.* **3–4** (2013) 93–97, <https://doi.org/10.1016/j.jcou.2013.07.008>.

- [120] Y. He, Y. Wang, L. Zhang, B. Teng, M. Fan, High-Efficiency Conversion of CO₂ to Fuel over ZnO/g-C₃N₄ Photocatalyst, *Appl. Catal. B* 168–169 (2015) 1–8, <https://doi.org/10.1016/j.apcatb.2014.12.017>.
- [121] Y. Wang, J. Zhao, T. Wang, Y. Li, X. Li, J. Yin, C. Wang, CO₂ Photoreduction with H₂O Vapor on Highly Dispersed CeO₂/TiO₂ Catalysts: Surface Species and Their Reactivity, *J. Catal.* 337 (2016) 293–302, <https://doi.org/10.1016/j.jcat.2015.12.030>.
- [122] E. Gong, S. Ali, C.B. Hiragond, H.S. Kim, N.S. Powar, D. Kim, H. Kim, In, S. Il. Solar Fuels: Research and Development Strategies to Accelerate Photocatalytic CO₂ Conversion into Hydrocarbon Fuels. *Energy and Environmental Science*, Royal Society of Chemistry, 2021, pp. 880–937, <https://doi.org/10.1039/d1ee02714j>.
- [123] A.G. Variar, M.S. Ramyashree, V.U. Ail, S.P. S, K. Sudhakar, M. Tahir, Influence of Various Operational Parameters in Enhancing Photocatalytic Reduction Efficiency of Carbon Dioxide in a Photoreactor: A Review, *J. Ind. Eng. Chem.* (2021) 19–47, <https://doi.org/10.1016/j.jiec.2021.04.017>.